

1 Interannual variability of the initiation of the phytoplankton 2 growing period in two French coastal ecosystems

3 Coline Poppeschi¹, Guillaume Charria¹, Anne Daniel², Romaric Verney³, Peggy Rimmelin-
4 Maury⁴, Michaël Retho⁵, Eric Goberville⁶, Emilie Grossteffan⁴, Martin Plus²

5 ¹Ifremer, Univ. Brest, CNRS, IRD, Laboratory for Ocean Physics and Satellite remote sensing (LOPS), IUEM,
6 29280 Brest, France.

7 ²Ifremer, DYNECO, Pelagic Ecology Laboratory (PELAGOS), 29280 Brest, France.

8 ³Ifremer, DYNECO, Hydrosedimentary Dynamics Laboratory (DHYSED), 29280 Brest, France.

9 ⁴OSU-European University Institute of the Sea (IUEM), UMS3113, 29280 Plouzané, France.

10 ⁵Ifremer, Morbihan-Pays de Loire Environment Resources Laboratory (LERMPL), 56100 Lorient, France.

11 ⁶Unité Biologie des Organismes et Ecosystèmes Aquatiques (BOREA), Muséum National d'Histoire Naturelle,
12 CNRS, IRD, Sorbonne Université, Université de Caen Normandie, Université des Antilles, Paris, France

13 *Correspondence to:* Coline Poppeschi (coline.poppeschi@ifremer.fr)

14 **Abstract.** Decadal time series of chlorophyll-*a* concentrations sampled at high and low frequencies are explored
15 to study climate-induced changes on the processes inducing interannual variations in the Initiation of the
16 Phytoplankton Growing Period (IPGP) in early spring. In this study, we specifically detail the IPGP in two
17 contrasting coastal temperate ecosystems under the influence of rivers highly rich in nutrients: the Bay of Brest
18 and the Bay of Vilaine. A large interannual variability in the IPGP is observed in both ecosystems in connection
19 with variations of environmental factors (available light depending from solar radiation, chlorophyll concentration
20 and turbidity - sea temperature - turbulence driven by currents, wind direction and intensity and tidal mixing -
21 nutrients from river flow). We show that the IPGP is delayed by around 30 days in 2019 in comparison with 2010.
22 *In situ* observations and a one-dimensional vertical model coupling hydrodynamics, biogeochemistry, and
23 sediment dynamics show that the IPGP generally depends on the interaction between several environmental
24 factors. IPGP is mainly conditioned, at the local scale, by sea surface temperature and available light conditions,
25 controlled by the turbidity of the system before first blooms. While both bays are hydrodynamically contrasted,
26 the processes that modulate IPGP are similar. In both bays, IPGP can be delayed by cold spells and flood events
27 at the end of winter if these extreme events last several days.

28
29 **Keywords**

30 Phytoplankton biomass, Long-term *in situ* observations, Coastal temperate ecosystems, Extreme events, Climate
31 change.

32 1 Introduction

33 Although studied for 70 years (Sverdrup, 1953), the optimal conditions that trigger the Initiation of
34 Phytoplankton Growing Period (IPGP) in ocean waters in early spring are not well understood (Sathyendranath *et al.*,
35 2015). Three main theories are proposed to date: the Critical Depth Hypothesis (Sverdrup, 1953), the Critical
36 Turbulence Hypothesis (Huisman *et al.*, 1999) and the Disturbance-Recovery Hypothesis (Banse, 1994;
37 Behrenfeld, 2010; Behrenfeld *et al.*, 2013). These hypotheses, determined with specific scales (e.g. mixed layer
38 depth dynamics and annual evolution) and ecosystems, are still regularly debated owing to the use of more efficient
39 models and new observation systems that allow the collection of large *in situ* datasets (Boss and Behrenfeld, 2010;
40 Rumyantseva *et al.*, 2019; Caracciolo *et al.*, 2021). Coastal waters remain highly dynamic and productive
41 ecosystems at the interface between land and sea and are distinguished from the waters of the open sea (e.g. Gohin
42 *et al.*, 2019; Liu *et al.*, 2019). Because coastal systems are directly influenced by anthropogenic inputs from rivers,
43 no nutrient limitation is observed in late winter. A myriad of factors and mechanisms can then affect the IPGP in
44 coastal areas (Townsend *et al.*, 1994; Cloern, 1996) but the incident light at the air/sea interface (Glé *et al.*, 2007)
45 and the sea surface temperature (Trombetta *et al.*, 2019) are the main forcings. Low water turbidity also plays a
46 major role and allows deeper light penetration (Iriarte and Purdie, 2004). This occurs by low vertical mixing
47 conditions in shallow waters (Ianson *et al.*, 2001), i.e. limited advective exchanges, weak wind (Tian *et al.*, 2011),
48 neap tide (Ragueneau *et al.*, 1996) and in absence of flooding events (Peierls *et al.*, 2012). Depending on the
49 morphology and hydrodynamics of coastal zones (estuaries, bays, lagoons), the importance of controlling factors

50 can be variable (Cloern, 1996). The variability of IPGP plays a major role on several biological compartments in
51 coastal ecosystems: change in the timing of IPGP can impact zooplankton and fish by inducing species
52 replacements (Sommer *et al.*, 2012), or phytoplankton itself by changing species composition or the succession of
53 species (Ianson *et al.*, 2001; Edwards and Richardson, 2004; Chivers *et al.*, 2020).

54 By amplifying or modifying environmental forcings, it is now well-documented that global climate
55 change may influence the IPGP in coastal areas (Smetacek and Cloern, 2008; Barbosa *et al.*, 2010; Pearl *et al.*,
56 2014; IPCC, 2021). Heat waves, as opposed to cold spells, have become more frequent in recent years and can
57 advance or delay the IPGP respectively (Gomez and Souissi, 2008). Wind storms, by inducing vertical mixing and
58 sediment resuspension, can have a significant effect on water turbidity which in turn limits light penetration and
59 therefore influences the IPGP. Floods, following heavier rainfall, may increase continental erosion, land-based
60 transfers and ultimately nutrient inputs to coastal ecosystems. Because coastal ecosystems are strongly influenced
61 by changes in land use, detecting long-term climate-induced signals is challenging (Krompkamp and Van
62 Engeland, 2010).

63 Our study is based on two geographically close but hydrodynamically different nearshore ecosystems:
64 (1) the Bay of Brest, a shallow semi-enclosed bay with well-mixed waters (Le Pape and Menesguen, 1997) and
65 (2) the Bay of Vilaine, a shallow open bay with long water residence times (Chapelle *et al.*, 1994). These two
66 coastal ecosystems are strongly impacted by anthropogenic pressures, such as intensive agriculture (Ragueneau *et al.*,
67 2018; Ratmaya *et al.*, 2019). The river influence induces waters highly rich in nutrients. Most studies dealing
68 with IPGP are mainly based on discrete water sampling (Iriarte *et al.*, 2004; Tian *et al.*, 2011) or modeling
69 (Townsend *et al.*, 1994; Philippart *et al.*, 2010). Only few studies investigate long-term high-frequency
70 observations (Gomez and Souissi, 2008; Iriarte and Purdie, 2004) to assess interannual variability of the IPGP and
71 to identify the triggering and controlling factors.

72 In this study, we aim to better understand interannual local changes in the IPGP in coastal temperate
73 ecosystems in the current context of global climate change over the last 20 years. We first detect and analyze the
74 temporal variability of the IPGP and we then quantify how environmental forcings influence its dynamics. To
75 detect and analyze IPGP in coastal environments, we develop a method, combining high-frequency decadal *in situ*
76 observations and modeling, based on a 1DV hydro-sedimentary and biogeochemical coupled numerical model.
77 The potential impact of hydro-meteorological extreme events, such as cold waves, flood events and wind bursts,
78 on the IPGP is then investigated.

80 2 Data and methods

82 2.1 Study areas

84 The study focuses on two northwestern French coastal temperate ecosystems, the Bay of Brest and the
85 Bay of Vilaine, which are both impacted by excessive nutrient inputs from watersheds, but exposed to different
86 hydrodynamic conditions.

87
88 The Bay of Brest is a semi-enclosed bay (180 km²) with 50% of the surface shallower than 5 m depth.
89 The Bay is connected with the Atlantic Ocean (Iroise sea) through a narrow and shallow strait. Tidal variation
90 reaches 8 m during spring tides, which represents an oscillating volume of 40 % of the high tide volume.
91 Freshwater inputs are essentially from the Aulne river (catchment area 1875 km², mean river flow 26 m³ s⁻¹), and
92 also from two smaller rivers, the Elorn (catchment area 385 km², mean river flow 6 m³ s⁻¹) and the Mignonne
93 (catchment area 111 km², mean river flow 1.5 m³ s⁻¹). Because of the macrotidal regime, the high nitrate
94 concentrations do not generate important green tides (Le Pape *et al.*, 1997) and the strong decreases in the Si:N
95 and Si:P ratios did not exhibit dramatic phytoplankton community shifts from diatoms to non-siliceous species in
96 spring (Del Amo *et al.*, 1997) according to the high Si recycling (Ragueneau *et al.*, 2002; Beucher *et al.*, 2004).

97
98 The Bay of Vilaine is a mesotidal open bay (69 km²) under the influence of the Vilaine (catchment area
99 10 500 km², mean river flow 70 m³ s⁻¹) and the Loire (catchment area 117 000 km², mean river flow 850 m³ s⁻¹)
100 river discharges, with tidal ranges varying between 4 and 6 m (Merceron, 1985). The Loire river plume tends to
101 spread northwestward with a dilution of 20- to 100-fold by the time it reaches the Bay of Vilaine (Menesguen *et al.*,
102 2018). The Vilaine river plume tends to spread throughout the bay before moving westward (Chapelle *et al.*,
103 1994). The water residence time varies seasonally between 10 and 20 days (Chapelle *et al.*, 1994). The water
104 circulation is mainly driven by tides, winds and river flows (Lazure and Jegou, 1998). This bay is well known as
105 one of the most sensitive European Atlantic coastal ecosystems to eutrophication (Menesguen *et al.*, 2019). The
106 Bay of Vilaine has undergone eutrophication over recent decades mainly due to high nutrient inputs from the
107 Vilaine and Loire rivers (Rossignol-Strick, 1985; Ratmaya *et al.*, 2019).

108 2.2 *In situ* observations

109

110 COAST-HF-Iroise (Rimmelin-Maury *et al.*, 2020) and COAST-HF-Molit (Retho *et al.*, 2020) are two high-
111 frequency monitoring buoys of the French national observation network COAST-HF¹ (Répécaud *et al.*, 2019;
112 Farcy *et al.*, 2019; Cocquempot *et al.*, 2019; Poppeschi *et al.*, 2021) located respectively in the Bay of Brest
113 (4.582°W; 48.357°N) and in the Bay of Vilaine (2.660°W; 47.434°N) (Fig. 1). COAST-HF-Iroise has been
114 operating in the strait between the Bay of Brest and the Iroise sea since 2000. COAST-HF-Molit buoy has been
115 sampling the plume of the Vilaine river since 2008. Buoys are deployed during the whole year except for COAST-
116 HF-Molit only available for part of the year prior to 2018 (from mid-February to early September, i.e. from day
117 50 to 250 for the period 2008-2017). Depending on the tide, the depth at the mooring sites ranges from 11 to 17 m
118 for both COAST-HF buoys. Environmental parameters (temperature, salinity, turbidity, dissolved oxygen and Chl-
119 *a* fluorescence) are measured at 2 m (COAST-HF-Iroise) and 1.3 m (COAST-HF-Molit) below the surface, every
120 20 and 60 minutes. The Chl-*a* fluorescence is measured by a Turner CYCLOPS-7 Sensor (precision \pm 5%) and
121 is considered as a proxy of phytoplankton biomass (unit FFU).

122 Sub-surface Chl-*a* concentrations are provided from two French marine monitoring networks, the SOMLIT
123 coastal observation network² and the REPHY (French Observation and Monitoring program for Phytoplankton
124 and Hydrology in coastal waters)³. They are collected bimonthly respectively at the SOMLIT-Brest (4.552°W;
125 48.358°N) and the REPHY-Loscolo (2.445°W; 47.496°N) stations which are close to the COAST-HF stations.
126 Chlorophyll-*a* concentrations are measured with either spectrophotometric or fluorimetric methods (Aminot and
127 K erouel, 2004).

128 Daily river flows are measured at gauging stations (French hydrology “Banque Hydro” database⁴), located
129 close to the main river mouths [Aulne-Gouezec (4.093°W; 48.205°N), Loire-Montjean (1.78°W; 47.106°N)]. The
130 Vilaine river flow is controlled by a dam, and data were provided by the Vilaine Public Territorial Basin
131 Organization⁵ (Fig. 1).

132 The tide gauge stations (Shom⁷) at Brest (4.495°W; 48.382°N) and Crouesty (2.895°W; 47.542°N) record the
133 sea level every minute.

134 Precipitation, air temperature, wind direction and intensity, and the solar flux data are retrieved every 6 minutes
135 from two meteorological stations from the M et eo-France observation network⁶: Guipavas (4.410°W; 48.440°N)
136 and Vannes-S en e (2.425°W; 47.362°N) (Fig. 1). The solar flux can be used here as a proxy for subsurface PAR
137 (Photosynthetically Available Radiation).

138 2.3 MARS3D-1DV modeling experiments

139 2.3.1 MARS3D-1DV model

140

141 A 1DV (one-dimensional vertical) model configuration is implemented to simulate changes in biogeochemical
142 variables due to hydrodynamics and sediment dynamics in both bays.

143

144 The hydrodynamical model is based on the MARS3D (3D hydrodynamics Model for Applications at Regional
145 Scale) code (Lazure and Dumas, 2008). This model is a primitive equation model with a free surface and uses the
146 Boussinesq and hydrostatic pressure assumptions. Here, we use the 1DV configuration of the model, with 10
147 vertical sigma levels for 15 m depth. The time step is 30 s.

148 The sediment model (MUSTANG - Le Hir *et al.*, 2011; Grasso *et al.*, 2015; Mengual *et al.*, 2017) is designed
149 to simulate the transport and changes in different sediment mixtures. In the sediment, 50 layers (refined near the
150 surface) for a total thickness of 40 cm are implemented. Four sediment classes are considered: muds (diameter 10
151 μm), fine sand (diameter 100 μm), medium sand (diameter 200 μm) and coarse sand (diameter 400 μm). The
152 sediment dynamics (transport in the water column, exchanges at the water/sediment interface, erosion/deposition

¹ www.coast-hf.fr, data available on www.coriolis-cotier.org

² <https://somlit.fr>

³ <https://doi.org/10.17882/47428>

⁴ www.hydro.eaufrance.fr/

⁵ <https://www.eptb-vilaine.fr/>

⁶ <https://donneespubliques.meteofrance.fr/>

⁷ <http://data.shom.fr>

153 processes) are driven by an advection/dispersion equation for each sediment class (refer to Le Hir et al., 2011 for
154 a detailed description of the sediment model).

155 The biogeochemical model BLOOM (Biogeochemical Coastal Ocean Model) is derived from the ECO-
156 MARS model (Cugier *et al.*, 2005; Ménesguen *et al.*, 2019) adding major processes of early diagenesis. Nitrogen,
157 phosphorus, and silica cycles are studied considering four nutrients, respectively nitrate, ammonium, soluble
158 reactive phosphorus, silicic acid (sorption/desorption of phosphate on suspended sediment and
159 precipitation/dissolution of phosphate with iron processes are also included). The model is also represented by
160 three phytoplankton classes (microphytoplankton, dinoflagellates, pico-nano-phytoplankton), two zooplankton
161 classes (micro- and meso-zooplankton), and exchanges at the water/sediment interface and inside the sediment
162 compartment.

163 2.3.2 MARS3D-1DV model sensitivity experiments

164
165 These three models (hydrodynamical, sediment and biogeochemical) are coupled online during simulations
166 and allow the nutrient and phytoplankton dynamics in both bays to be reproduced. The simulation for the Bay of
167 Brest does not include nutrient inputs from the sediment because it is considered to be negligible around the
168 COAST-HF-Iroise station.

169 Dissolved and particulate variables are defined in the water column and in the sediment. Initial values for both
170 bays are uniform over the initial vertical profile (Table 1) and are based on a 3D realistic coupled simulation during
171 the year 2015 the 15th of February extracted at the position of COAST-HF-Iroise for the Bay of Brest and at the
172 position of COAST-HF-Molit station for the Bay of Vilaine (Plus *et al.*, 2021).

173
174 To evaluate the sensitivity of the biogeochemical dynamics to environmental conditions, sensitivity
175 experiments are then performed using the coupled MARS3D/BLOOM/MUSTANG 1DV model configuration. All
176 simulations are started at the end of winter (15th February) and run until the end of the year. The range of values
177 used in the sensitivity experiments are derived from the minimum and maximum observed *in situ* data. Each
178 parameter is tested with a constant value for the whole simulation.

179
180 Three parameters are individually explored in both bays:

- 181 - The air temperature in sensitivity experiments ranges from 4 to 14°C and is controlled by the intensity of
182 solar radiations. Air temperature represents the main controlling parameter of Sea Surface Temperature in
183 the 1DV model. This parameter drives the radiative fluxes in the model and then constrains the SST.
- 184 - Wind intensity effect on the IPGP is explored for values between 0 and 10 m s⁻¹. In the 1DV model, wind
185 is a source of vertical mixing in the simulation.
- 186 - The Cloud Coverage (CC) sensitivity experiments ranged in value between 0 and 100% CC. This
187 parameter is a driver of Photosynthetic Available Radiation (PAR) in the ocean. For the formulation of
188 radiative fluxes in the 1DV MARS3D model, 100% cloud coverage allows an inflow of 38% of the total
189 solar radiation in the water column. Each individual experiment is associated with a constant CC applied
190 to the seasonal solar radiation.

191 As the sediment plays a role on the light penetration and acts as an active source of nutrients mainly in the Bay
192 of Vilaine, the mud erosion rate (values between $2 \cdot 10^{-5}$ and $2 \cdot 10^{-7}$ kg m⁻² s⁻¹) is explored only in that bay (sand
193 erosion rate fixed to 0.0001 kg m⁻² s⁻¹). For the sensitivity experiments, it drives a mass of sediment eroded
194 and resuspended and a bottom input of nutrients in the water column.

195
196 A second set of experiments is conducted combining the effect of these environmental parameters in order to
197 explore the cumulative or opposite effect on the IPGP. The upper and lower bounds of the range of
198 environmental parameters are taken into account. Experiments are detailed in Table 5.

199 2.4 Data processing

200 2.4.1 Chl-*a* fluorescence data

201
202 To analyze high-frequency time series of *in situ* Chl-*a* fluorescence, the Quenching effect (Lehmuskero
203 *et al.*, 2018), a decrease in fluorescence in the presence of light (Fig. 2), is removed by analyzing only night-time
204 data as reported in Carberry *et al.* (2019). Chl-*a* fluorescence data are studied on a daily basis, i.e. averaged from
205 10 pm to 5 am. Years with less than 75% of valid data (i.e. 2005, 2006, 2008, 2009 and 2018 in the Bay of Brest)
206 are not considered.

207

208 2.4.2 Detection of the IPGP

209

210 We apply methods from the literature (Kromkamp *et al.*, 2010; Philippart *et al.*, 2010; Brody *et al.*, 2013)
211 to calculate annual IPGP values (not shown). Kromkamp *et al.* (2010) set an arbitrary beginning and end of the
212 phytoplankton growing period at 20% and 80% of the cumulative Chl-*a* fluorescence measured from January 1st
213 to December 31st. Similarly, Brody *et al.* (2013) consider a threshold of 5% above the yearly median chlorophyll.
214 Philippart *et al.* (2010) considers the beginning of the growing period as the maximum daily difference in Chl-*a*
215 fluorescence.

216 Because we obtain unrealistic IPGP dates from our dataset when using the methods proposed by Kromkamp *et al.*
217 (2010 - i.e. too late IPGP); Brody *et al.* (2013 - i.e. too early IPGP) and Philippart *et al.* (2010 - i.e. multiple
218 IPGP), we propose an alternative detection method based on discontinuities of the Chl-*a* fluorescence signal (Fig.
219 3): daily FFU slopes are calculated based on a linear regression over a +/-2 day window for each day, from 1st
220 January to 31st December, and each year. The IPGP date is identified when the slope exceeds a threshold value,
221 defined as the median of the daily slopes, for the first time in the year for at least 20 days. The end of the
222 phytoplankton growing period is determined when the slope stabilizes below the threshold for at least 20 days for
223 the last time in the year. The cumulative Chl-*a* fluorescence corresponds to the duration of the growing period.

224 2.4.3 Pattern of the phytoplankton growing period

225

226 The k-means method (Hartigan and Wong, 1979) is used to characterize the annual patterns of the
227 phytoplankton growing period.

228 We exclude the year 2013 from the analysis of the Bay of Vilaine because of a large number of missing
229 data. When the interval over which consecutive data are missing is no longer than one week, we perform a linear
230 interpolation to replace the missing data. A 5-day running average is applied to the Chl-*a* fluorescence signal and
231 the data are then normalized by the maximum value. We analyze Chl-*a* fluorescence every year for 150 days after
232 the IPGP.

233 Time series from both bays are merged before application of the k-means and the number of clusters (or
234 centroids) is set at 2 to distinguish the dominant patterns of the phytoplankton growth period at both sites. The use
235 of a larger number of clusters is investigated and does not produce a pattern representing a large number of
236 observed growing periods.

237 2.4.4 Detection of extreme events

238

239 The peak over threshold method (see Oliver *et al.*, 2018 and Poppeschi *et al.*, 2021 for further details) is
240 used to detect hydro-meteorological extreme events such as cold waves, flood events and wind bursts. An event is
241 considered as extreme if values are higher than a given statistical threshold for at least 3 consecutive days. In the
242 present study, the 90-percentile threshold is selected to detect floods and wind bursts and the 10-percentile to
243 detect cold waves. Seasonal anomalies are calculated over at least 20 years, by subtracting raw data from the winter
244 average value (cold spells) or from the spring average value (wind bursts and floods).
245

246 3. Results

247 3.1 Characterization of the phytoplankton growing period

248

249 The high-frequency Chl-*a* fluorescence time series at both sites show an intense seasonal cycle with low
250 values from November to February and high values from March to October (Fig. 4). Focusing on the period from
251 2010 to 2019 in the Bay of Brest, the minimum Chl-*a* fluorescence is observed during the years 2012 and 2013
252 and does not exceed 7 FFU. In contrast, years such as 2010, 2014, 2015 or 2019 show Chl-*a* fluorescence values
253 above 15 FFU but can be up to 20 FFU. In the Bay of Vilaine, a similar seasonal pattern is observed with higher
254 values reaching 50 FFU in 2013. Small (< 20 FFU) and high (> 35 FFU) Chl-*a* fluorescence amplitude are observed
255 occasionally (in 2014 and 2017 and in 2013 and 2016, respectively). The Chl-*a* fluorescence is higher, almost
256 double, in the Bay of Vilaine compared to the Bay of Brest with a mean cumulative Chl-*a* fluorescence around
257 580 FFU and 360 FFU, respectively (Table 2). The high phytoplankton biomass of the Bay of Vilaine is
258 corroborated by the concentrations measured by low-frequency observation programs (SOMLIT and REPHY).

259 The phytoplankton growing period ranges from approximately March 10th to September 30th in both regions
260 (Table 2). The average duration of the phytoplankton growing period is 179 days in the Bay of Vilaine and 200
261 days in the Bay of Brest (Table 2). The phytoplankton growing period is characterized by successive blooms,
262 whose number and intensity are variable from year to year (Fig. 4).

263
264 The main patterns of the phytoplankton growing period are identified by the two clusters (Fig. 5). Cluster 0
265 includes the phytoplankton growing period with two successive marked blooms in early spring and in summer,
266 the intensity of the second bloom being highly variable. Cluster 1 is characterized by a plateau during the two first
267 months of the phytoplankton growing period. Most of the patterns of the Bay of Vilaine are in cluster 0 while those
268 of the Bay of Brest are in cluster 1 (Table 3). The years that stand out in the Bay of Brest (2002, 2010, 2014)
269 correspond to years with the highest cumulative *Chl-a* fluorescence (≥ 450 FFU). The atypical years in the Bay
270 of Vilaine (2011, 2017 and 2019) show the lowest cumulative *Chl-a* fluorescence (≤ 450 FFU).

271 3.2 Variability of the Initiation of the Phytoplankton Growing Period (IPGP)

272
273 Calculations performed to determine the IPGP for high- and low-frequency data yield comparable results (Fig.
274 6). The mean differences between the IPGP calculated with the high and low-frequency data are 5 and 8 days for
275 the Bay of Brest and the Bay of Vilaine, respectively. A difference of only 4 and 6 days between the model
276 simulations (reference year = 2015) and the high-frequency *in situ* data is observed in the Bay of Brest and the
277 Bay of Vilaine, respectively.

278
279 A decadal variability of the IPGP is recorded from mid-February to mid-April in both ecosystems (day 50 to
280 day 102 in the Bay of Brest and day 53 to day 93 in the Bay of Vilaine; Fig. 6). In the Bay of Brest, early IPGPs
281 (day < 53) are observed in 2010 and 2013 whereas late IPGP (day > 93) are observed in 2001, 2017 and 2019. In
282 the Bay of Vilaine, the earliest IPGP is detected in 2012 (day 53) and the latest in 2019 (day 93).

283
284 The variability of IPGP in the Bay of Brest shows two linear trends (Fig. 6a), with a decrease of 52 days from
285 2001 to 2010 (observed in both high- and low-frequency datasets), followed by an increase (+48 days) from 2011
286 to 2019, a decline also observed in the Bay of Vilaine (Fig. 6b). Over the period 2011-2019, the IPGP is shifted
287 towards a later date by +3.5 days per year in the Bay of Vilaine and +3.7 days per year in the Bay of Brest.

288 3.3 Analysis of environmental conditions driving the IPGP

289 3.3.1 Impact of environmental conditions on the IPGP

290
291 We next quantify the influence of environmental drivers on the date of IPGP (Fig. 7). These drivers
292 represent the major limiting factors of the phytoplankton growth and comprise input of nutrients (river flow), PAR
293 (incident light), Sea Surface Temperature - SST - (air temperature, incident light) and turbidity in the water column
294 (river flow, wind intensity).

295
296 The median values of the environmental drivers observed at the date of each annual IPGP are very close
297 in both bays (Table 4) : temperate SST (10 °C), weak wind (3 m.s⁻¹), a medium PAR (1360 W m⁻²), a low turbidity
298 (7 NTU) and a weak tidal amplitude (semi-amplitude of 1.6 m in the Bay of Brest and 0.9 m in the Bay of Vilaine).
299 The IPGP occurs mainly during neap tides, at 68 % and 77 % in the Bay of Brest and in the Bay of Vilaine,
300 respectively. The river flow is low during the IPGP with a runoff of 46 m³ s⁻¹ for the Aulne, 96 m³ s⁻¹ for the
301 Vilaine and 1196 m³ s⁻¹ for the Loire.

302
303 To assess how environmental drivers may impact (i.e. advance or delay) the IPGP, we focus on the 15
304 days before the mean day of the IPGP (day 68) and of each annual IPGP. The considered 15 days length is related
305 to the typical water residence time in both bays (Frere *et al.*, 2017; Poppeschi *et al.*, 2021 for the Bay of Brest -
306 Chapelle *et al.*, 1994; Ratmaya *et al.*, 2019 for the Bay of Vilaine).

307 The earliest IPGP dates (IPGP < day 55) are associated with earlier occurrence of favorable
308 environmental conditions than the other years. Earliest IPGP which occurred before day 55 are in 2010 and 2013
309 in the Bay of Brest and in 2012 in the Bay of Vilaine (Fig. S1f, 7c - S2a). Early IPGP between day 55 to 60, also
310 associated with favorable environmental conditions, are found in 2002 and 2016 in the Bay of Brest (Fig. S1b,
311 S1j).

312 In the same way, the latest IPGP dates (IPGP > day 90) are associated with unfavorable environmental
313 conditions until the date of the IPGP. Latest IPGP occurring after day 90 are observed in 2001, 2003, 2017 and
314 2019 in the Bay of Brest and in 2019 in the Bay of Vilaine (Fig. S1a,c,k,l - S2g). For example, the delay detected
315 in 2017 in both bays is due to strong wind and a lack of PAR until the day of IPGP (Fig. S1k - Fig. S2e). Late
316 IPGP between day 70 to 90 are recorded in 2004, 2007 and 2012 in the Bay of Brest, and in 2014, 2017 and 2018
317 in the Bay of Vilaine (Fig. S1d,e,g, 7d - S2e,f).

318
319 The interannual variability of the date of the IPGP is therefore not controlled by a unique environmental
320 driver. When the values of the environmental drivers responsible for the IPGP (Table 4) are compared to the mean
321 values of the environmental drivers over a period of 30 days around the IPGP (Table S1), threshold values are
322 observed in both bays: river flow is lower than usual (between 10 and 30 m³ s⁻¹), temperature is close to the
323 expected value (10°C), wind is weak (0.5 to 1.5 m s⁻¹), PAR is stronger (>300 W m⁻²), and turbidity is low (about
324 1.5 NTU). IPGP starts around day 68 (± 3 days) on average (Fig. 7a,b).

325 3.3.2 Modeling the importance of the environmental drivers

326
327 The relative contribution of each environmental driver on the IPGP is determined by MARS-1DV simulations
328 starting on February 1st (Fig. 8). Environmental drivers tested in the model are controlling:

- 329 - the sea temperature - explored in the model by perturbing air temperature (as a controlling driver in the
330 model of the Sea Surface Temperature evolution),
- 331 - the level of water turbulence - through wind intensity,
- 332 - the available light - controlled by Cloud Coverage (CC, as a sea surface PAR proxy) and turbidity (erosion
333 rate as a proxy) limiting light penetration in the water column.

334 Model results show that early IPGP are associated with air temperature higher than 9 °C (resulting in a SST higher
335 than 8 °C), low wind intensity, weak CC and low turbidity. Environmental drivers responsible for early or late
336 IPGP are similar in both bays. Air temperature is the main driver with a potential deviation from the mean IPGP
337 of 25 days in the Bay of Brest and 40 days in the Bay of Vilaine (Fig. 8). Wind, CC and turbidity have a lower
338 impact on the IPGP (around 6 days in the Bay of Brest and 13 days in the Bay of Vilaine). In the Bay of Vilaine,
339 the environmental drivers can simulate later IPGP than in the Bay of Brest.

340
341 In the Bay of Brest (Fig. 8a), only the air temperature variations have a real impact on the IPGP. If the air
342 temperature is low (< 8°C), the IPGP is not triggered before day 74 (Table 5, Exp 1). If the air temperature is high
343 (>13°C), the IPGP can start on day 49 (Table 5, Exp 2).

344 In the Bay of Vilaine, the air temperature and the erosion rate are the two main drivers impacting the IPGP
345 (Fig. 8b). Similarly to the Bay of Brest, if the air temperature is low (< 6°C), the IPGP is late and appears only
346 after day 80 (Table 5, Exp 1). If temperature is equal or above 13°C, the IPGP is early and appears on day 45
347 (Table 5, Exp 2). If the erosion rate is low (2.10⁻⁷ kg m⁻² s⁻¹), then the IPGP takes place on day 76 (Table 5, Exp
348 7). If the erosion rate is high (2.10⁻⁵ kg m⁻² s⁻¹), the IPGP occurs late after day 87 (Table 5, Exp 8).

349 The variations of wind and CC induce weaker shifts in the date of the IPGP, i.e. about one week at the most
350 (Table 5, Exp 3,4,5,6). However, wind and CC can still explain variations of IPGP. For example, early IPGPs, in
351 2010 in the Bay of Brest and in 2012 in the Bay of Vilaine, due to low wind conditions (around 2 m s⁻¹, Fig. S2a
352 - S1f) are observed in *in situ* measurements and also confirmed by the model (Fig. 8b).

353
354 The combined effect of the environmental factors can also be explored from the MARS-1DV model
355 simulations (Fig. 9). The modeling conditions (hereafter called “Exp”) are detailed in Table 5 and compared to the
356 mean IPGP date (day 68).

357 The simulations confirm the observations, late IPGP correspond to the most extreme unfavorable combined
358 environmental values (temperature of 4°C, wind intensity of 10 m s⁻¹, CC of 100% and erosion rate of 2.10⁻⁵ kg
359 m⁻² s⁻¹ - Exp A). In the Bay of Brest and the Bay of Vilaine, IPGP occurs 9 days (i.e. twice as late as for any
360 individual driver simulation) and 64 days later respectively. Late IPGP can also be linked to the combined effect
361 of only two factors such as: “temperature and wind” and “temperature and CC” with a delay of 5 and around 22
362 days respectively (Exp B,C). In contrast, no delay is observed for the combination “wind and CC” (Exp D) in both
363 bays.

364 Same as previously, early IPGP are found in the simulations as in the observations when conditions correspond to
365 a high temperature (14°C), no wind intensity and CC, and a low erosion rate (2.10⁻⁷ kg m⁻² s⁻¹) - Exp K. All the
366 combined scenarios permit the occurrence of an earlier IPGP (by at least 5 additional days) compared to
367 experiments that consider a single modified parameter.

369 This analysis enables environmental parameters to be classified with respect to their impact on the IPGP.
370 In both bays, the temperature appears to be the key factor driving the IPGP. By combining the environmental
371 drivers, the IPGP can occur even later or earlier than with a single forcing. In both bays, the combination of wind
372 and CC has no impact on the IPGP, which occurs near the median day (Exp D and N). The extreme couplings of
373 Exp A,E,F,G,J delay the date of IPGP later than detected in the observations for the Bay of Vilaine. All simulations
374 show a higher impact on the date of IPGP in the Bay of Vilaine than in the Bay of Brest (Fig. 9, Table 5).

375 **3.4 Impact of extreme hydro-meteorological events on the IPGP**

376 **3.4.1 Cold spells**

377 The impact of cold spells on the IPGP is simulated with the MARS-1DV model based on two criteria: (i)
378 the period of occurrence of the event, set in mid- or end February, (ii) the duration and intensity of the cold spell,
379 which can be either short and weak (8 days, 7°C) or long and intense (20 days, 5°C) (Fig. 10).

380 In both bays, when the cold spell appears in mid-February, the IPGP is not impacted. However, it is
381 delayed by about 15 days when occurring at the end of February. The duration of the cold spell, when longer than
382 15 days, also has an impact on the IPGP, with a delay of 13 and 12 days in the Bay of Brest and in the Bay of
383 Vilaine, respectively.

384 Eight cold spells are detected in February in both bays between 2001 and 2019. In 2011, both sites are
385 impacted simultaneously with cold spells. Long cold spells (30 days) are observed in 2009 and 2018, leading to
386 an anomaly of more than -1.9°C.

387 The cold spell observed in 2018 in the Bay of Vilaine may explain the later IPGP. There is no change in
388 the IPGP in 2011 and 2013, despite the cold spell, the period of occurrence being too early during winter 2011,
389 and the duration too short in 2013 (only 10 days).

390 In the Bay of Brest, the cold spells in 2003 and 2004 may explain the delay of the IPGP (respectively
391 days 93 and 85). The presence of long and intense cold spells in 2010 and 2011 do not shift the IPGP (days 50 and
392 67) because they occur too early (before day 20).

393 **3.4.2 Wind bursts**

394
395 Based on our model simulations, the wind bursts that occur during at least three continuous days have no
396 impact on the IPGP in both bays, whatever the duration, the period and the intensity (+/- 1 day). In the Bay of
397 Vilaine, only one wind event is detected in 2018 (3 days long and 6 m.s⁻¹). In the Bay of Brest, several events are
398 detected, but no significant impact is observed on the IPGP.

399 **3.4.3 Flood events**

400
401 River floods can delay the IPGP by resuspending sediment in the water column and therefore limiting
402 light penetration in the water column. Inputs of nutrients have no impact during the late winter period because
403 nutrient concentrations are maximal, with no limitation on phytoplankton growth. Flood events are analyzed with
404 observation data collected in the month prior to the IPGP date because the 1DV modeling approach does not allow
405 the sensitivity to hydrological events to be simulated (*i.e.* it is necessary to simulate horizontal advection
406 processes).

407
408 In the Bay of Brest, the impact of flood events depends on their duration and intensity: when the flood
409 exceeds 15 days, a delay in the IPGP is detected. Shorter and more intense floods (> 300 m³ s⁻¹) do not impact the
410 IPGP.

411
412 In the Bay of Vilaine, only two flood events are observed close to the IPGP date in 2014 and 2015. The
413 2015 flood event, which is 10 days longer and more intense (> 100 m³ s⁻¹) than the 2014 one, delays the IPGP date
414 by 10 days.
415

416 4 Discussion

417 4.1 Comparison of the phytoplankton growing period in both bays

418
419 Despite their contrasting hydrodynamics (*e.g.* Petton *et al.*, 2020; Poppeschi *et al.*, 2021; Lazure and
420 Jegou, 1998; Ratmaya *et al.*, 2019; Menesguen *et al.*, 2019), the median dates of the start and the end of the
421 phytoplankton growing period are the same in the Bay of Brest and in the Bay of Vilaine whether they are
422 calculated from high- and low- frequency datasets and from model simulations. The phytoplankton growing period
423 occurs from March to September and lasts about 190 days in both bays. This concordance is related to a similar
424 seasonality of the environmental drivers.

425 The observed cumulative fluorescence is almost double in the Bay of Vilaine compared with the Bay of
426 Brest. This difference in the amount of chlorophyll produced in surface waters from both bays is also recorded by
427 the low-frequency observation programs and by satellite observations (Menesguen *et al.*, 2019). It can be explained
428 by the difference of the hydrodynamics and the influence of different watersheds. The Bay of Brest is a semi-
429 enclosed bay with a macro-tidal regime influenced by two local rivers (Aulne and Elorn) whereas the Bay of
430 Vilaine has a weaker tidal regime, is open on the continental shelf and is widely influenced by a large river (Loire
431 river).

432 Two different patterns of the phytoplankton growing period are identified by the k-means classification
433 in both bays. The flattened, weak and long bloom highlighted in the Bay of Brest can be explained by assuming
434 that nutrients are not limiting the phytoplankton growth during spring. The maintenance of the diatom succession
435 throughout spring since the 1980's (Quéguiner 1982; Del Amo *et al.*, 1997) can be explained by the combination
436 of increasing N and P loads, intense Si recycling and a macrotidal regime (Ragueneau *et al.*, 2019). The
437 phytoplankton growing period in the bay of Vilaine is characterized by several successive peaks including two
438 main ones. Nutrients here drive the seasonal evolution of the phytoplankton growing period through periods of
439 nutrient-limited conditions. These fluctuations are governed by phosphorus and nitrate loads from Vilaine and
440 Loire rivers (Ratmaya *et al.*, 2019), but probably also by the stoichiometry of recycled elements in the water and
441 at the water-sediment interface (Ratmaya *et al.*, 2022). However, at the beginning of the phytoplankton growing
442 period (IPGP), the system is not nutrient limited in terms of nitrate, phosphorus and silicates.

443 444 445 4.2 Identification of the environmental conditions supporting the IPGP

446
447 The method that we developed to detect IPGP on both high-frequency and low-frequency *in situ*
448 observations shows comparable results and detects similar initiation dates for some years, while a time lag between
449 high- and low-frequency observations can be observed for other years. This difference is mainly explained by the
450 difference in the sampling frequency. The late deployment of the buoy in the Bay of Vilaine (*i.e.* not deployed
451 until mid-February before 2018) can also explain some differences between both sites. High-frequency data
452 provide a more accurate detection of the day of the IPGP, while an uncertainty of about ± 7 days is observed with
453 low-frequency observations. This comparison between high- and low-frequency based IPGP detection highlights
454 the sensitivity of sampling strategy in the observation of phytoplankton growing periods (Bouman *et al.*, 2005;
455 Serre-Fredj *et al.*, 2021) related to the response of the ecosystem within a few hours after an environmental change
456 (Lefort and Gasol, 2014; Thyssen *et al.*, 2008).

457
458 The modeled IPGP, based on the year 2015, is coherent with high-frequency observations (around 5 days
459 of difference between modeled and observed IPGP). Considering the idealized framework for modeling
460 computations (1DV model instead of a realistic 3D model configuration), the agreement between observations and
461 simulations validates the 1DV approach to explore IPGP dynamics. With the 1DV configuration, the vertical
462 dynamics in the water column, coupled with biogeochemistry and sediment dynamics are well reproduced.
463 Atmospheric forcings and interactions with the bottom layer are the main environmental drivers. The full range of
464 impacts related to the horizontal advection (*e.g.* in considered regions, rivers advected plumes can change the
465 hydrodynamics and the biogeochemical contents) are not evaluated, however. In the Bay of Brest and in the Bay
466 of Vilaine, such advected sources exist (*e.g.* Poppeschi *et al.*, 2021; Lazure and Jegou, 1998) but inputs from rivers
467 are not main drivers of the IPGP in nutrient-rich environments. Nutrient loads advected by rivers may impact the
468 phytoplankton community later during the growing period rather than at IPGP (*e.g.* Ratmaya *et al.*, 2019).

469
470 We characterize similar environmental conditions in both bays as the IPGP is mainly driven and limited
471 by similar local conditions. The ideal temperature ($> 10^{\circ}\text{C}$) and PAR (1300 W m^{-2}) for the IPGP are in agreement
472 with those from previous studies conducted in similar coastal ecosystems (*e.g.* Glé *et al.*, 2007; Townsend *et al.*,
473 1994; Trombetta *et al.*, 2019). Neap tidal conditions, weak wind (lower than 3 m s^{-1}) and weak river flow can also
474 play a positive role to observe earlier IPGP according to the previous study of Ragueneau *et al.*, 1996.

475 As also shown in the German Bight (Tian *et al.*, 2011), wind intensity is a driver of turbidity in the water column
476 which inhibits phytoplankton growth. The impact of wind direction on the IPGP is estimated to be negligible.
477 Local changes in those features (temperature, incident radiation, tidal conditions, wind conditions and river flow)
478 induce differences in detected IPGP. Indeed, in this coastal temperate ecosystem, we observe that the beginning
479 of the growing period is limited by light (controlled by incident radiation, turbidity at this season), and water
480 temperature. The IPGP also occurs during low vertical mixing conditions.
481

482 The comparison of the individual importance of each environmental driver shows that temperature and
483 light penetration are the key environmental drivers in both bays. Similarly in the North Sea, Wiltshire *et al.* (2015)
484 highlight the importance of the light availability in the timing and intensity of the spring bloom. Similarly, too
485 high turbidity (due to sediment resuspension) can also limit the production and delay IPGP in the bay of Vilaine.
486 Similar limitations are observed in the German Bight (Tian *et al.*, 2009) or along the UK South Coast (Iriarte and
487 Purdie, 2004). The combined effect of surface incident radiation and turbidity can amplify the delay of the IPGP.
488 However, with the existence of minimum mandatory conditions, an earlier IPGP can not be observed or modeled,
489 except if thresholds are reached earlier (e.g. warmer temperature earlier during the year).
490

491 4.3 Interannual evolutions of the IPGP

492
493 The IPGP in these two bays shows a strong interannual variability with initiation dates varying from late
494 winter to spring. A mean difference of 50 days between the earliest and latest IPGP dates is observed. Each year
495 has a different date of IPGP related to different environmental conditions. However, the beginning of the
496 phytoplankton growing period is always dominated in both bays by the same centric diatoms, genera *Chaetoceros*
497 and *Skeletonema*, whose abundance varies from year to year depending on climatic conditions (REPHY, 2021).
498

499 The earliest IPGP are observed and related to favorable environmental conditions early in the year. For
500 example, the IPGP can occur before day 50, associated with exceptionally weak wind and river flow in addition
501 to a sufficient PAR and nearly-optimal temperature of around 10°C (e.g. 2010 in the Bay of Brest and 2012 in the
502 Bay of Vilaine). But if the environmental conditions are not favorable (e.g. 2017 and 2019 in both bays), the IPGP
503 is delayed. This can be due to a strong wind during several days (not a single wind burst) and a weak PAR and
504 sometimes also because of turbidity events limiting the light penetration.

505 However, the reason to have early or late IPGP is not always the same. Late IPGP can be due to low
506 temperature conditions rather than a strong wind or a lack of PAR as seen previously (e.g. 2003 in Bay of Brest).
507 Also, the IPGP can be different from one bay to another in the same year, almost half of the years studied from
508 2012 to 2016. For example, the 2012 IPGP is early in the Bay of Vilaine (day 53) while it is late in the Bay of
509 Brest (day 80), related to strong wind activity and low PAR. This difference between the two bays indicates a
510 local, not regional, effect of the processes affecting the IPGP.

511 The analysis of the IPGP over the last two decades has highlighted its evolution through two trends, one
512 per decade. The IPGP occurs earlier each year until 2010 when the trend is reversed. At a larger scale, this change
513 in trends is not directly observed for the same years. For example, using hourly data, Hunter-Cervera *et al.* (2016)
514 show earlier blooms of picophytoplankton on the New England Shelf during 2003-2012 due to warming spring
515 periods, and later blooms in 2013-2015 for cooler spring temperatures. The similarity between these observations
516 and those found here in our study on the other side of the Atlantic basin for a slightly later breaking year (2012
517 instead of 2010) suggests a large-scale impact of the warming waters in spring. On the eastern part of the Atlantic,
518 we also know that 2010 was an atypical year, with an important accumulation of phytoplankton biomass as
519 observed by Bedford *et al.* (2020) on the North-West European shelf. However, limited indicators do not allow
520 conclusions to be drawn regarding the impact of large-scale forcings on observed shifts in phytoplankton blooms.
521

522 As the climate warms, earlier phytoplankton blooms are expected (Friedland *et al.*, 2018) but not later
523 IPGP as observed in our study regions. However, the mechanisms that trigger blooms in coastal ecosystems -
524 especially eutrophic ones - are not similar to the processes that influence blooms in the open ocean. For example,
525 by investigating long-term (1975-2005) daily data, Wiltshire *et al.* (2008) observe later phytoplankton blooms in
526 the German bight, but with no link to global warming. Henson *et al.* (2018) model a bloom shift of 5 days per
527 decade from 2006 to 2025, with later blooms. A possible explanation may involve the lower spring sea surface
528 temperatures, as observed in recent years (Hunter-Cervera *et al.* 2016), which could cause a delay of the IPGP.
529 We do not detect significant trends in environmental conditions over the last 20 years at either site, and therefore
530 do not establish direct links with the trends observed in the IPGP timing. In the southern California Bight, similar
531 changes in IPGP are observed from 1983 to 2000, but no link with environmental drivers has been identified (Kim
532 *et al.*, 2009).
533

534 4.4 Extreme events

535
536 We show that a cold spell is likely to delay the IPGP if it occurs at the end of winter (after 20th February)
537 or/and if the cold spell lasts long enough (> 15 days). This is in accordance with the study of Gomez and Souissi
538 (2008) in the English Channel where cold spells can affect the date of IPGP by increasing the water column mixing.
539 In both bays, the drop in temperature related to the cold spell prevents the IPGP. Cold spells may also drive local
540 patterns by influencing the phytoplankton communities (Gomez and Souissi, 2008; Schlegel *et al.*, 2021).

541 Flood events have an influence on the phytoplankton biomass when they occur in spring due to the supply
542 of nutrients. When they occur in late winter, nutrients are already at their maximum. The impact of floods on IPGP
543 is consequent only if they are at least 15 days long. This scheme is also observed by Saeck *et al.* (2013) along a
544 river-estuary-bay continuum and explained by a shortened water residence time and a limited light due to flood-
545 induced turbidity in the coastal zone.

546 No relationship is observed between wind events and IPGP in both bays because they are weakly stratified
547 contrary to open seas (*i.e.* Black Sea, Mikaelyan *et al.*, 2017). In coastal stratified regions (e.g. under the influence
548 of river plumes), strong wind and tidal mixing can enhance the mixing and break down stratification thus
549 distributing phytoplankton (Joordens *et al.*, 2021). During the IPGP, except during floods, both regions are weakly
550 stratified and are then less sensitive to combined wind/tidal short events.

551 **5 Conclusions**

552
553 This study provides a new understanding of the IPGP dynamics in coastal temperate areas by using both
554 high and low-frequency *in situ* data, in combination with simulations from a 1DV model. Strong similarities are
555 found in both bays. An important interannual variability of the IPGP is observed, with a trend towards a later IPGP
556 over the last decade (2010-2020). We quantify the importance of environmental conditions on the IPGP. When
557 we compare observed IPGP with favorable environmental conditions and following sensitivity experiments with
558 the 1DV model, water temperature and turbidity (limiting light penetration in the water column) appear as the
559 main drivers explaining interannual IPGP variability. The IPGP is a complex mechanism, usually triggered by
560 more than one environmental parameter. The analysis of the influence of extreme events reveals that cold spells
561 and floods have a strong impact by delaying the IPGP when episodes are long enough and occur after winter. No
562 effect of wind bursts is detected.

563 While this study shows comparable IPGP dynamics when based on 1DV model simulations or *in situ*
564 observations, we will next investigate the effect of a fully realistic hydrodynamics (including horizontal and
565 vertical advections; mixing processes; remote sources of nutrients from rivers) on phytoplankton dynamics using
566 a 3D model. We will focus on exploring the variability of phytoplankton communities during IPGP to assess
567 whether community change is occurring, as observed in other studies and for other ecosystems (Ianson *et al.*, 2001;
568 Edwards and Richardson, 2004; Chivers *et al.*, 2020). When interannual evolutions in the phytoplankton growth
569 are explored, the detection and the understanding of harmful algal bloom dynamics can also be addressed based
570 on similar approaches. Further studies will be dedicated to the simulation of the coastal ecosystem in the future
571 based on numerical simulation based on climate scenarios. The investigation of other contrasting coastal
572 environments will allow us to better understand and anticipate the expected impact of global change on coastal
573 phytoplankton dynamics.

574 **Author contributions**

575 CP, GC, AD, RV, PR-M and EGo conceptualized the study. PR-M, EGr and MR collected data. MP and GC
576 developed the model configuration. CP, GC, AD and RV drafted the first versions of the paper. CP carried out all
577 the analyses and wrote the final version of the paper. All authors contributed to the discussions and revisions of
578 the study.

579 **Acknowledgements**

580 We would like to acknowledge COAST-HF (<http://www.coast-hf.fr>), SOMLIT ([http://somlit.epoc.u-](http://somlit.epoc.u-bordeaux1.fr)
581 [bordeaux1.fr](http://somlit.epoc.u-bordeaux1.fr)) and REPHY (<https://doi.org/10.17882/47248>) national observing networks, for providing data flux
582 readily available. COAST-HF and SOMLIT are components of the National Research Infrastructure ILICO. We
583 would like to thank the Shom for tidal data and also Météo-France for wind and solar flux products. We also thank
584 Dr Claire Labry for fruitful discussions and Dr Sally Close for her proofreading.

585 **Financial support**

586 This study is part of the State-Region Plan Contract ROEC supported in part by the European Regional
587 Development Funds and the COXTCLIM project funded by the Loire-Brittany Water Agency, the Brittany region
588 and Ifremer.

589 **References**

590
591 Aminot, A., and Kerouel, R.: Hydrologie des écosystèmes marins. Paramètres et analyses, Editions de l'Ifremer,
592 336 p., ISBN 2-84433-133-5, 2004.

593
594 Banse, K.: Grazing and zooplankton production as key controls of phytoplankton production in the open
595 ocean, *Oceanography*, 7(1), 13-20, <https://www.jstor.org/stable/43925524>, 1994.

596 Barbosa, A., Domingues, R., and Galvão, H.: Environmental forcing of phytoplankton in a Mediterranean estuary
597 (Guadiana estuary, south-western Iberia): A decadal study of anthropogenic and climatic influences, *Estuaries and*
598 *Coasts*, doi:10.1007/s12237-009-9200-x, 2010.

599 Bedford, J., Ostle, C., Johns, D. G., Atkinson, A., Best, M., Bresnan, E., ... and McQuatters-Gollop, A.: Lifeform
600 indicators reveal large-scale shifts in plankton across the North-West European shelf, *Global Change Biology*,
601 26(6), 3482-3497, doi:10.1111/gcb.15066, 2020.

602 Behrenfeld, M. J.: Abandoning Sverdrup's critical depth hypothesis on phytoplankton blooms, *Ecology*, 91(4),
603 977-989, doi:10.1890/09-1207, 2010.

604
605 Behrenfeld, M. J., Doney, S. C., Lima, I., Boss, E. S., and Siegel, D. A.: Annual cycles of ecological disturbance
606 and recovery underlying the subarctic Atlantic spring plankton bloom, *Global biogeochemical cycles*, 27(2), 526-
607 540, doi:10.1002/gbc.20050, 2013.

608
609 Beucher, C., Treguer, P., Corvaisier, R., Hapette, A. M., and Elskens, M.: Production and dissolution of biosilica,
610 and changing microphytoplankton dominance in the Bay of Brest (France), *Marine Ecology Progress Series*, 267,
611 57-69, doi:10.3354/meps267057, 2004.

612
613 Boss, E., and Behrenfeld, M.: In situ evaluation of the initiation of the North Atlantic phytoplankton bloom,
614 *Geophysical Research Letters*, 37(18), doi:10.1029/2010GL044174, 2010.

615
616 Bouman, H., Platt, T., Sathyendranath, S., and Stuart, V.: Dependence of light-saturated photosynthesis on
617 temperature and community structure, *Deep Sea Research Part I: Oceanographic Research Papers*, 52(7), 1284-
618 1299, doi:10.1016/j.dsr.2005.01.008, 2005.

619
620 Brody, S. R., Lozier, M. S., and Dunne, J. P.: A comparison of methods to determine phytoplankton bloom
621 initiation, *Journal of Geophysical Research, Oceans*, 118(5), 2345-2357, doi:10.1002/jgrc.20167, 2013.

622
623 Caracciolo, M., Beaugrand, G., Hélaouët, P., Gevaert, F., Edwards, M., Lizon, F., ... and Goberville, E.: Annual
624 phytoplankton succession results from niche-environment interaction, *Journal of Plankton Research*, 43(1), 85-
625 102, doi:10.1093/plankt/fbaa060, 2021.

626
627 Chapelle, A., Lazure, P., and Ménesguen, A.: Modelling eutrophication events in a coastal ecosystem. Sensitivity
628 analysis, *Estuarine, Coastal and Shelf Science*, 39(6), 529-548, doi:10.1016/S0272-7714(06)80008-9, 1994.

629
630 Chivers, W. J., Edwards, M., and Hays, G. C.: Phenological shuffling of major marine phytoplankton groups over
631 the last six decades, *Diversity and Distributions*, 26(5), 536-548, doi:10.1111/ddi.13028, 2020.

632
633 Cloern, J. E.: Phytoplankton bloom dynamics in coastal ecosystems: a review with some general lessons from
634 sustained investigation of San Francisco Bay, California, *Reviews of Geophysics*, 34(2), 127-168,
635 doi:10.1029/96RG00986, 1996.

636

- 637 Cocquempot, L., Delacourt, C., Paillet, J., Riou, P., Aucan, J., Castelle, B., Charria, G., Claudet, J., Conan, P.,
638 Coppola, L., Hocdé, R., Planes, S., Raimbault, P., Savoye, N., Testut, L., and Vuillemin, R.: Coastal Ocean and
639 Nearshore Observation: A French Case Study, *Frontiers in Marine Science*, 6(324), 1-17,
640 doi:10.3389/fmars.2019.00324, 2019.
- 641
- 642 Cook, P. L., Holland, D. P., and Longmore, A. R.: Effect of a flood event on the dynamics of phytoplankton and
643 biogeochemistry in a large temperate Australian lagoon, *Limnology and Oceanography*, 55(3), 1123-1133,
644 doi:10.4319/lo.2010.55.3.1123, 2010.
- 645
- 646 Cugier, P., Billen, G., Guillaud, J. F., Garnier, J., and Ménesguen, A.: Modelling the eutrophication of the Seine
647 Bight (France) under historical, present and future riverine nutrient loading, *Journal of Hydrology*, 304(1-4), 381-
648 396, doi:10.1016/j.jhydrol.2004.07.049, 2005.
- 649
- 650 Del Amo, Y., Le Pape, O., Tréguer, P., Quéguiner, B., Ménesguen, A., and Aminot, A.: Impacts of high-nitrate
651 freshwater inputs on macrotidal ecosystems. I. Seasonal evolution of nutrient limitation for the diatom-dominated
652 phytoplankton of the Bay of Brest (France), *Marine Ecology Progress Series*, 161, 213-224, doi:10.5194/bg-16-
653 1361-2019, 1997.
- 654
- 655 Edwards, M., and Richardson, A. J.: Impact of climate change on marine pelagic phenology and trophic
656 mismatch, *Nature*, 430(7002), 881-884, doi:10.1038/nature02808, 2004.
- 657
- 658 Farcy, P., Durand, D., Charria, G., Painting, S.J., Tamminem, T., Collingridge, K., Grémare, A.J., Delauney, L.,
659 and Puillat, I.: Toward a European coastal observing network to provide better answers to science and to societal
660 challenges; the JERICO research infrastructure, *Frontiers in Marine Science*, 6, 1–13,
661 doi:10.3389/fmars.2019.00529, 2019.
- 662
- 663 Frère, L., Paul-Pont, I., Rinnert, E., Petton, S., Jaffré, J., Bihannic, I., Soudant, P., Lambert, C. and Huvet, A.:
664 Influence of environmental and anthropogenic factors on the composition, concentration and spatial distribution
665 of microplastics : a case study of the Bay of Brest (Brittany, France), *Environ. Pollut*, 225, 211–222,
666 doi:10.1016/j.envpol.2017.03.023, 2017.
- 667
- 668 Friedland, K. D., Mouw, C. B., Asch, R. G., Ferreira, A. S. A., Henson, S., Hyde, K. J., ... and Brady, D. C.:
669 Phenology and time series trends of the dominant seasonal phytoplankton bloom across global scales, *Global
670 Ecology and Biogeography*, 27(5), 551-569, doi:10.1111/geb.12717, 2018.
- 671
- 672 Glé, C., Del Amo, Y., Bec, B., Sautour, B., Froidefond, J. M., Gohin, F., Maurer, D., Plus, M., Laborde, P., and
673 Chardy, P.: Typology of environmental conditions at the onset of winter phytoplankton blooms in a shallow
674 macrotidal coastal ecosystem, Arcachon Bay (France), *Journal of plankton research*, 29(11), 999-1014,
675 doi:10.1093/plankt/fbm074, 2007.
- 676
- 677 Gohin, F., Van der Zande, D., Tilstone, G., Eleveld, M. A., Lefebvre, A., Andrieux-Loyer, F., Blauw, A. N.,
678 Bryère, P., Devreker, D., Garnesson, P., Hernández Fariñas, T., Lamaury, Y., Lampert, L., Lavigne, H., Menet-
679 Nedelec, F., Pardo, S., and Saulquin, B.: Twenty years of satellite and in situ observations of surface chlorophyll-
680 a from the northern Bay of Biscay to the eastern English Channel. Is the water quality improving ? *Remote Sensing
681 of Environment*, 233(September), 111343, doi:10.1016/j.rse.2019.111343, 2019.
- 682
- 683 Gomez, F., and Souissi, S.: The impact of the 2003 heat wave and the 2005 cold wave on the phytoplankton in the
684 north-eastern English Channel, *Comptes Rendues Biologies*, 331(9), 678-685, doi:10.1016/j.crv.2008.06.005,
685 2008.
- 686
- 687 Grasso F., Le Hir P., and Bassoullet P.: Numerical modelling of mixed-sediment consolidation, *Ocean Dynamics*,
65(4), 607– 616, doi:10.1007/s10236-015-0818-x, 2015.
- 688
- 689 Hartigan, J., and Wong, M.: Algorithm AS 136: A K-Means Clustering Algorithm. *Journal of the Royal Statistical
690 Society, Series C (Applied Statistics)*, 28:1, 100-108, doi:2346830, 1979.
- 691
- 692 Henson, S. A., Cole, H. S., Hopkins, J., Martin, A. P., and Yool, A.: Detection of climate change-driven trends in
phytoplankton phenology, *Global Change Biology*, 24(1), e101-e111, doi:10.1111/gcb.13886, 2018.

693
694 Huisman, J. E. F., van Oostveen, P., and Weissing, F. J.: Critical depth and critical turbulence: two different
695 mechanisms for the development of phytoplankton blooms, *Limnology and oceanography*, 44(7), 1781-1787,
696 doi.org/10.4319/lo.1999.44.7.1781, 1999.

697
698 Hunter-Cevera, K. R., Neubert, M. G., Olson, R. J., Solow, A. R., Shalapyonok, A., and Sosik, H. M.:
699 Physiological and ecological drivers of early spring blooms of a coastal phytoplankter, *Science*, 354(6310), 326-
700 329, doi:10.1126/science.aaf8536, 2016.

701
702 Husson, B., Hernández-Fariñas, T., Le Gendre, R., Schapira, M., and Chapelle, A.: Two decades of Pseudo-
703 nitzschia spp. blooms and king scallop (*Pecten maximus*) contamination by domoic acid along the French Atlantic
704 and English Channel coasts: Seasonal dynamics, spatial heterogeneity and interannual variability, *Harmful*
705 *Algae*, 51, 26-39, doi:10.1016/j.hal.2015.10.017, 2016.

706
707 Ianson, D., Pond, S., and Parsons, T.: The spring phytoplankton bloom in the coastal temperate ocean: growth
708 criteria and seeding from shallow embayments, *Journal of oceanography*, 57(6), 723-734,
709 doi.org/10.1023/A:1021288510407, 2001.

710
711 IPCC: Summary for Policymakers. In: *Climate Change 2021: The Physical Science Basis. Contribution of*
712 *Working Group I to the Sixth Assessment Report of the Intergovernmental Panel on Climate Change* [Masson-
713 Delmotte, V., P. Zhai, A. Pirani, S. L. Connors, C. Péan, S. Berger, N. Caud, Y. Chen, L. Goldfarb, M. I. Gomis,
714 M. Huang, K. Leitzell, E. Lonnoy, J.B.R. Matthews, T. K. Maycock, T. Waterfield, O. Yelekçi, R. Yu and B. Zhou
715 (eds.)], Cambridge University Press, In Press, 2021.

716
717 Iriarte, A., and Purdie, D. A.: Factors controlling the timing of major spring bloom events in an UK south coast
718 estuary, *Estuarine, Coastal and Shelf Science*, 61(4), 679-690, doi:10.1016/j.ecss.2004.08.002, 2004.

719
720 Joordens, J. C. A., Souza, A. J., & Visser, A.: The influence of tidal straining and wind on suspended matter and
721 phytoplankton distribution in the Rhine outflow region. *Continental Shelf Research*, 21(3), 301-325,
722 doi:10.1016/S0278-4343(00)00095-9, 2001.

723
724 Kromkamp, J. C., and Van Engeland, T.: Changes in phytoplankton biomass in the western Scheldt estuary during
725 the period 1978-2006, *Estuaries and Coasts*, 33(2), 270–285, doi:10.1007/s12237-009-9215-3, 2010.

726
727 Kim, H. J., Miller, A. J., McGowan, J., and Carter, M. L.: Coastal phytoplankton blooms in the Southern California
728 Bight, *Progress in Oceanography*, 82(2), 137-147, doi:10.1016/j.pocean.2009.05.002, 2009.

729
730 Lazure, P., and Dumas, F.: An external–internal mode coupling for a 3D hydrodynamical model for applications
731 at regional scale (MARS), *Advances in water resources*, 31(2), 233-250, doi:10.1016/j.advwatres.2007.06.010,
732 2008.

733
734 Lazure, P., and Jégou, A. M.: 3D modelling of seasonal evolution of Loire and Gironde plumes on Biscay Bay
735 continental shelf, *Oceanologica acta*, 21(2), 165-177, doi:10.1016/S0399-1784(98)80006-6, 1998.

736
737 Lefort, T., and Gasol, J. M.: Short-time scale coupling of picoplankton community structure and single-cell
738 heterotrophic activity in winter in coastal NW Mediterranean Sea waters, *Journal of plankton research*, 36(1),
243-258, doi:10.1093/plankt/fbt073, 2014.

739
740 Le Hir P., Cayocca F., and Waeles B.: Dynamics of sand and mud mixtures: A multiprocess-based modelling
strategy, *Continental Shelf Research*, 31(10), S135– S149, doi:10.1016/j.csr.2010.12.009, 2011.

741
742 Lehmuskero, A., Skogen Chauton, M., and Boström, T.: Light and photosynthetic microalgae: A review of
743 cellular- and molecular-scale optical processes, *Progress in Oceanography*, 168(September), 43–56,
doi:10.1016/j.pocean.2018.09.002, 2018.

744
745 Le Pape, O., and Menesguen, A.: Hydrodynamic prevention of eutrophication in the Bay of Brest (France), a
746 modelling approach, *Journal of Marine Systems*, 12(1-4), 171-186, doi:10.1016/S0924-7963(96)00096-6, 1997.

- 747 Liu, X., Dunne, J. P., Stock, C. A., Harrison, M. J., Adcroft, A., and Resplandy, L.: Simulating water residence
748 time in the coastal ocean: A global perspective, *Geophysical Research Letters*, 46(23), 13910-13919, doi:
749 10.1029/2019GL085097, 2019.
- 750
751 Ménesguen, A., Dussauze, M., and Dumas, F.: Designing optimal scenarios of nutrient loading reduction in a
752 WFD/MSFD perspective by using passive tracers in a biogeochemical-3D model of the English Channel/Bay of
753 Biscay area, *Ocean & Coastal Management*, 163, 37-53, doi:10.1016/j.ocecoaman.2018.06.005, 2018.
- 754
755 Ménesguen, A., Dussauze, M., Dumas, F., Thouvenin, B., Garnier, V., Lecornu, F., and Répécaud, M.: Ecological
756 model of the Bay of Biscay and English Channel shelf for environmental status assessment part 1: Nutrients,
757 phytoplankton and oxygen, *Ocean Modelling*, 133, 56-78, doi.org/10.1016/j.ocemod.2018.11.002, 2019.
- 758
759 Mengual B., Le Hir P., Cayocca F., and Garlan T.: Modelling fine sediment dynamics: Towards a common erosion
law for fine sand, mud and mixtures, *Water*, 9, 564, doi:10.3390/w9080564, 2017.
- 760
761 Mikaelyan, A., Chasovnikov, V., Kubryakov, A., and Stanichny, S.: Phenology and drivers of the winter-spring
762 phytoplankton bloom in the open Black Sea: The application of Sverdrup's hypothesis and its refinements,
Progress in Oceanography, 151, 163-176, doi:10.1016/j.pocean.2016.12.006, 2017.
- 763
764 Monchevaa, S., Gotsis-Skretasb, O., Pagoub, K., and Krasteva, A.: Phytoplankton Blooms in Black Sea and
765 Mediterranean Coastal Ecosystems Subjected to Anthropogenic Eutrophication: Similarities and
766 Differences, *Estuarine, Coastal and Shelf Science*, 53, 281-295, doi:10.1006/ecss.2001.0767, 2001.
- 767
768 Oliver, E., Donat, M., Burrows, M., Moore, P., Smale, D., Alexandra, L., Benthuisen, J., Feng, M., Sen Gupta, A.,
769 Hobday, A., Holbrook, N., Perkins-Kirkpatrick, S., Scannell, H., Straub, S. and Wernberg, T.: Longer and more
770 frequent marine heatwaves over the past century, *Nature communications*, 9 :1324, doi:10.1038/s41467-018-
771 03732-9, 2018.
- 772
773 Paerl, H. W., Hall, N. S., Peierls, B. L., and Rossignol, K. L.: Evolving paradigms and challenges in estuarine and
774 coastal eutrophication dynamics in a culturally and climatically stressed world, *Estuaries and coasts*, 37(2), 243-
775 258, doi.org/10.1007/s12237-014-9773-x, 2014.
- 776
777 Peierls, B. L., Hall, N. S., and Paerl, H. W.: Non-monotonic responses of phytoplankton biomass accumulation to
778 hydrologic variability: a comparison of two coastal plain North Carolina estuaries, *Estuaries and coasts*, 35(6),
779 1376-1392, doi.org/10.1007/s12237-012-9547-2, 2012.
- 780
781 Petton, S., Pouvreau, S., and Dumas, F. Intensive use of Lagrangian trajectories to quantify coastal area dispersion,
782 *Ocean Dynamics*, 70(4), 541-559, doi.org/10.1007/s10236-019-01343-6, 2020.
- 783
784 Philippart, C. J. M., van Iperen, J. M., Cadée, G. C., and Zuur, A. F.: Long-term field observations on seasonality
785 in chlorophyll-a concentrations in a shallow coastal marine ecosystem, the Wadden Sea, *Estuaries and Coasts*,
786 33(2), 286–294, doi:10.1007/s12237-009-9236-y, 2010.
- 787
788 Plus, M., Thouvenin, B., Andrieux, F., Dufois, F., Ratmaya, W., Souchu, P. Diagnostic étendu de l'eutrophisation
789 (DIETE). Modélisation biogéochimique de la zone Vilaine-Loire avec prise en compte des processus
790 sédimentaires. Description du modèle Bloom (Biogeochemical Coastal Ocean Model). RST/LER/MPL/21.15.
791 <https://archimer.ifremer.fr/doc/00754/86567/>, 2021.
- 792
793 Poppeschi, C., Charria, G., Goberville, E., Rimmelin-Maury, P., Barrier, N., Petton, S., Unterberger, M.,
794 Grossteffan, E., Repeccaud, M., Quémener, L., Le Roux, J.-F., and Tréguer, P.: Unraveling salinity extreme events
795 in coastal environments: a winter focus on the bay of Brest, *Frontiers in Marine Science*, 8,
796 705403, doi:10.3389/fmars.2021.705403, 2021.
- 797
798 Quéguiner, B., and Tréguer, P.: Studies on the Phytoplankton in the Bay of Brest (Western Europe), Seasonal
799 Variations in Composition, Biomass and Production in Relation to Hydrological and Chemical Features (1981—
800 1982), *Botanica Marina*, 27, 449-459, 1984.
- 801
802 Ragueneau, O., Quéguiner, B. and Tréguer, P.: Contrast in biological responses to tidally-induced vertical mixing
803 for two macrotidal ecosystems of western Europe, *Estuarine, Coastal and Shelf Science*, 42, 645-665,
doi:10.1006/ecss.1996.0042, 1996.

804
805 Ragueneau, O., Chauvaud, L., Leynaert, A., Thouzeau, G., Paulet, Y. M., Bonnet, S., Lorrain, A., Grall, J.,
806 Corvaisier, R., Le Hir, M., Jean, F., and Clavier, J.: Direct evidence of a biologically active coastal silicate pump:
807 ecological implications, *Limnology and Oceanography*, 47(6), 1849-1854, doi.org/10.4319/lo.2002.47.6.1849,
808 2002.
809
810 Ragueneau, O., Raimonet, M., Mazé, C., Coston-Guarini, J., Chauvaud, L., Danto, A., Grall, J., Jean, F., Paulet
811 Y.-M., and Thouzeau, G.: The impossible sustainability of the Bay of Brest ? Fifty years of ecosystem changes,
812 interdisciplinary knowledge construction and key questions at the science-policy-community interface, *Frontiers*
813 *in Marine Science*, 5, 124, doi.org/10.3389/fmars.2018.00124, 2018.
814
815 Ratmaya, W., Soudant, D., Dalmon-Monviola, J., Plus, M., Cochennec-Laureau, N., Goubert, E., Andrieux-Loyer,
816 F., Barillé, L. and Souchu, P.: Reduced phosphorus loads from the Loire and Vilaine rivers were accompanied by
817 increasing eutrophication in the Vilaine Bay (south Brittany, France), *Biogeosciences*, 16:1361-1380,
818 doi:10.5194/bg-16-1361-2019, 2019.
819
820 Ratmaya, W., Laverman, AM., Rabouille, C., Akbarzadeh, Z., Andrieux-Loyer, F., Barillé, L., Barillé, A-L., Le
821 Merrer, Y., and Souchu, P.: Temporal and spatial variations in benthic nitrogen cycling in a temperate macro-tidal
822 coastal ecosystem : Observation and modeling, *Continental Shelf Research*, doi:10.1016/j.csr.2022.104649, 2022.
823
824 Répécaud, M., Quemener, L., Charria, G., Pairaud, I., Rimmelin, P., Claquin, P., Jacqueline, F., Lefebvre, A.,
825 Facq, J.V., Retho, M., and Verney, R.: National observation infrastructure: an example of a fixed-platforms
826 network along the French Coast: COAST HF, OCEANS IEE, pp. 1-6, doi:10.1109/OCEANSE.2019.8867451,
827 2019.
828
829 REPHY: French Observation and Monitoring program for Phytoplankton and Hydrology in coastal waters,
830 REPHY dataset - French Observation and Monitoring program for Phytoplankton and Hydrology in coastal waters.
831 Metropolitan data, SEANOE, doi:10.17882/47248, 2021.
832
833 Retho, M., Quemener, L., Le Gall, C., Repecaud, M., Souchu, P., Gabellec, R. and Manach, S.: MOLIT Vilaine
834 data and metadata from Coriolis Data Centre, SEANOE, doi:10.17882/46529, 2020.
835
836 Rimmelin-Maury, P., Charria, G., Repecaud, M., Quemener, L., Beaumont, L. Guillot, A., Gautier, L., Prigent, S.,
837 Le Becque, T., Bihannic, I., Bonnat, A., Le Roux, J-F., Grossteffan, E., Devesa, J., and Bozec, Y.: Iroise buoys
838 data from Coriolis data center as core parameter support for Brest Bay and Iroise sea studies, SEANOE, 2020.
839
840 Rossignol-Strick, M.: A marine anoxic event on the Brittany coast, July 1982, *Journal of Coastal Research*, 11-
841 20, https://www.jstor.org/stable/4297005, 1985.
842
843 Rumyantseva, A., Henson, S., Martin, A., Thompson, A. F., Damerell, G. M., Kaiser, J., and Heywood, K. J.:
844 Phytoplankton spring bloom initiation: The impact of atmospheric forcing and light in the temperate North
845 Atlantic, Ocean. *Progress in oceanography*, 178, 102202, doi:10.1016/j.pocean.2019.102202, 2019.
846
847 Saeck, E. A., Hadwen, W. L., Rissik, D., O'Brien, K. R., and Burford, M. A.: Flow events drive patterns of
848 phytoplankton distribution along a river–estuary–bay continuum, *Marine and Freshwater Research*, 64(7), 655-
849 670, doi:10.1071/MF12227, 2013.
850
851 Sathyendranath, S., Ji, R., and Browman, H. I.: Revisiting Sverdrup's critical depth hypothesis, *ICES Journal of*
852 *Marine Science*, 72(6), 1892-1896, doi:10.1093/icesjms/fsv110, 2015.
853
854 Schlegel, R. W., Darmaraki, S., Benthuisen, J. A., Filbee-Dexter, K., and Oliver, E. C.: Marine cold-
855 spells, *Progress in Oceanography*, 198, 102684, doi.org/10.1101/2021.10.18.464880, 2021.
856
857 Serre-Fredj, L., Jacqueline, F., Navon, M., Izabel, G., Chasselin, L., Jolly, O., ... and Claquin, P.: Coupling high
858 frequency monitoring and bioassay experiments to investigate a harmful algal bloom in the Bay of Seine (French-
859 English Channel), *Marine Pollution Bulletin*, 168, 112387, doi:10.1016/j.marpolbul.2021.112387, 2021.
860

861 Smetacek, V., & Cloern, J. E.: On phytoplankton trends, *Science*, 319(5868), 1346-1348, doi:
862 10.1126/science.1151330, 2008.
863

864 Sommer, U., Adrian, R., De Senerpont Domis, L., Elser, J. J., Gaedke, U., Ibelings, B., Jeppesen, E., Lürling, M.,
865 Molinero, J. C., Mooij, W. M., van Donk, E., and Winder, M.: Beyond the Plankton Ecology Group (PEG) model:
866 mechanisms driving plankton succession, *Annual review of ecology, evolution, and systematics*, 43, 429-448,
867 doi:10.1146/annurev-ecolsys-110411-160251, 2012.
868

869 Stockwell, J. D., Doubek, J. P., Adrian, R., Anneville, O., Carey, C. C., Carvalho, L., ... and Wilson, H. L.: Storm
870 impacts on phytoplankton community dynamics in lakes, *Global change biology*, 26(5), 2756-2784,
871 doi:10.1111/gcb.15033, 2020.
872

873 Sverdrup, H.: On vernal blooming of phytoplankton, *Conseil Exp. Mer*, 18, 287-295, 1953.
874

875 Thyssen, M., Tarran, G. A., Zubkov, M. V., Holland, R. J., Grégori, G., Burkill, P. H., and Denis, M.: The
876 emergence of automated high-frequency flow cytometry: revealing temporal and spatial phytoplankton variability,
877 *Journal of plankton research*, 30(3), 333-343, doi:10.1093/plankt/fbn005, 2008.
878

879 Tian, T., Merico, A., Su, J., Staneva, J., Wiltshire, K., and Wirtz, K.: Importance of resuspended sediment
880 dynamics for the phytoplankton spring bloom in a coastal marine ecosystem, *Journal of Sea Research*, 62(4), 214-
881 228, doi:10.1016/j.seares.2009.04.001, 2009.
882

883 Tian, T., Su, J., Flöser, G., Wiltshire, K., and Wirtz, K.: Factors controlling the onset of spring blooms in the
884 German Bight 2002–2005: light, wind and stratification, *Continental Shelf Research*, 31(10), 1140-1148,
885 doi:10.1016/j.csr.2011.04.008, 2011.
886

887 Townsend, D. W., Cammen, L. M., Holligan, P. M., Campbell, D. E., and Pettigrew, N. R.: Causes and
888 consequences of variability in the timing of spring phytoplankton blooms, *Deep Sea Research Part I:
889 Oceanographic Research Papers*, 41(5-6), 747-765, doi:10.1016/0967-0637(94)90075-2, 1994.
890

891 Trombetta, T., Vidussi, F., Mas, S., Parin, D., Simier, M., and Mostajir, B.: Water temperature drives
892 phytoplankton blooms in coastal waters, *PloS one*, 14(4), e0214933, doi:10.1371/journal.pone.0214933, 2019.
893

894 Wiltshire, K. H., Malzahn, A. M., Wirtz, K., Greve, W., Janisch, S., Mangelsdorf, P., ... and Boersma, M.:
895 Resilience of North Sea phytoplankton spring bloom dynamics: An analysis of long-term data at Helgoland
896 Roads, *Limnology and Oceanography*, 53(4), 1294-1302, doi:10.4319/lo.2008.53.4.1294, 2008.
897

898 Wiltshire, K. H., Boersma, M., Carstens, K., Kraberg, A. C., Peters, S., and Scharfe, M.: Control of phytoplankton
899 in a shelf sea: determination of the main drivers based on the Helgoland Roads Time Series, *Journal of Sea
900 Research*, 105, 42-52, doi:10.1016/j.seares.2015.06.022, 2015.
901
902
903
904
905
906
907
908
909
910
911
912
913
914
915
916
917
918
919
920
921
922

923
924
925
926
927
928
929
930
931
932
933
934
935
936
937
938
939
940
941
942
943
944
945
946
947
948
949
950
951
952
953
954
955
956
957
958
959
960

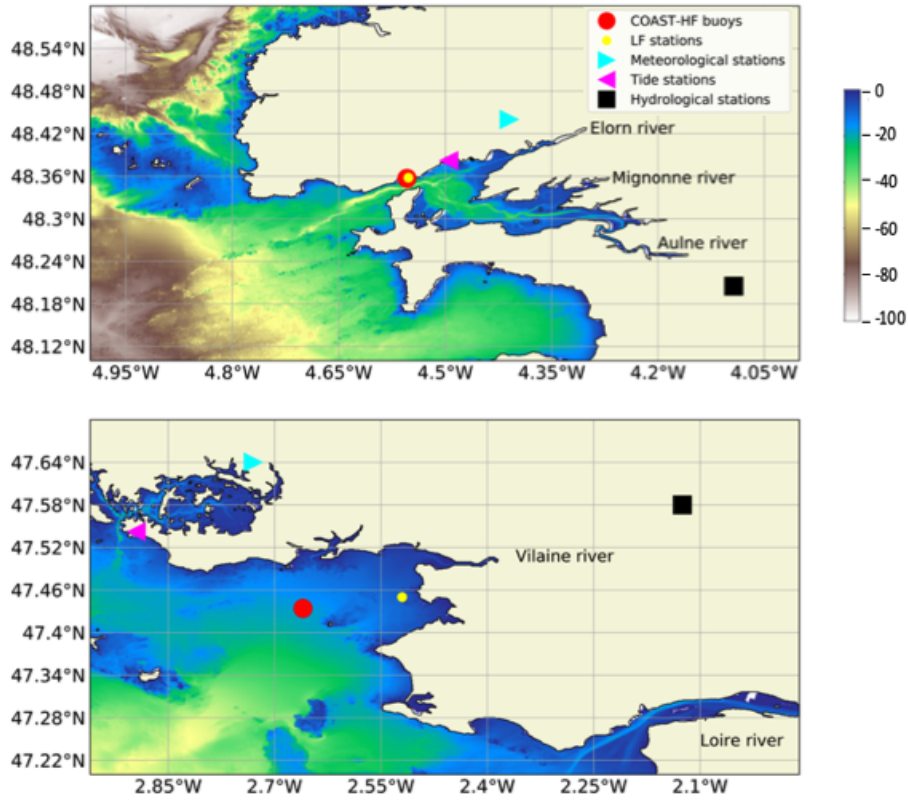


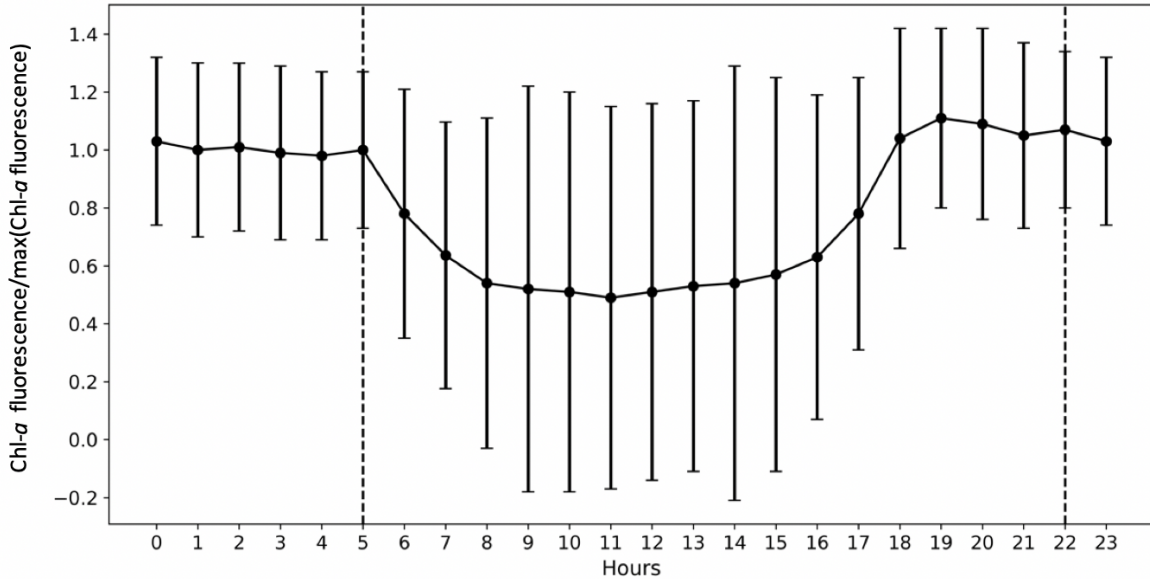
Figure 1: Location of the sampling sites: COAST-HF-Iroise and COAST-HF-Molit buoys (red circles); SOMLIT-Brest and REPHY-Loscolo sampling stations (yellow circles); Brest and Crouesty tide gauge stations (blue triangles); Guipavas and Vannes-Séné meteorological stations (purple triangles); hydrological stations of the Aulne and Vilaine rivers (black squares) with the Loire station off the map.

Parameters	Bay of Brest	Bay of Vilaine
Dissolved O ₂ ($mg L^{-1}$)	9	10
Mesozooplankton ($\mu mol N L^{-1}$)	0.05	0.1
Microzooplankton ($\mu mol N L^{-1}$)	0.05	0.05
Dinoflagellates ($\mu mol N L^{-1}$)	0.05	0.1
Diatoms ($\mu mol N L^{-1}$)	0.5	0.5
Soluble reactive phosphorus ($\mu mol L^{-1}$)	0.5	0.8
Silicic acid ($\mu mol L^{-1}$)	10	30
Nitrate ($\mu mol L^{-1}$)	16	30
Ammonium ($\mu mol L^{-1}$)	0.5	0.25
Coarse sand ($g L^{-1}$)	0	0
Fine sand ($g L^{-1}$)	0	0

Mud ($g L^{-1}$)	0.03	0.05
--------------------	------	------

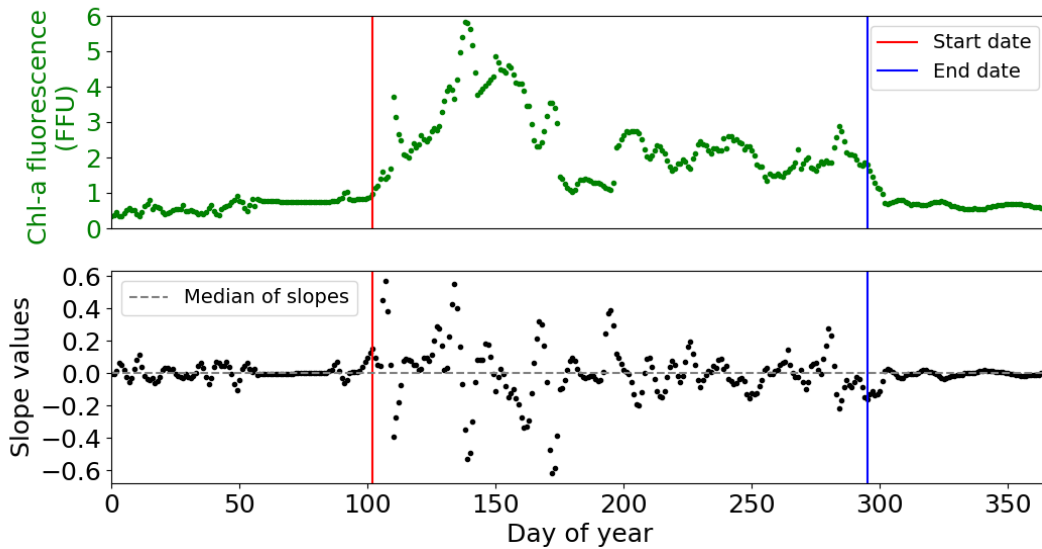
961
962
963
964

Table 1: Initial conditions in the water column for the MARS-1DV model for the beginning of the simulation on the February 15th.



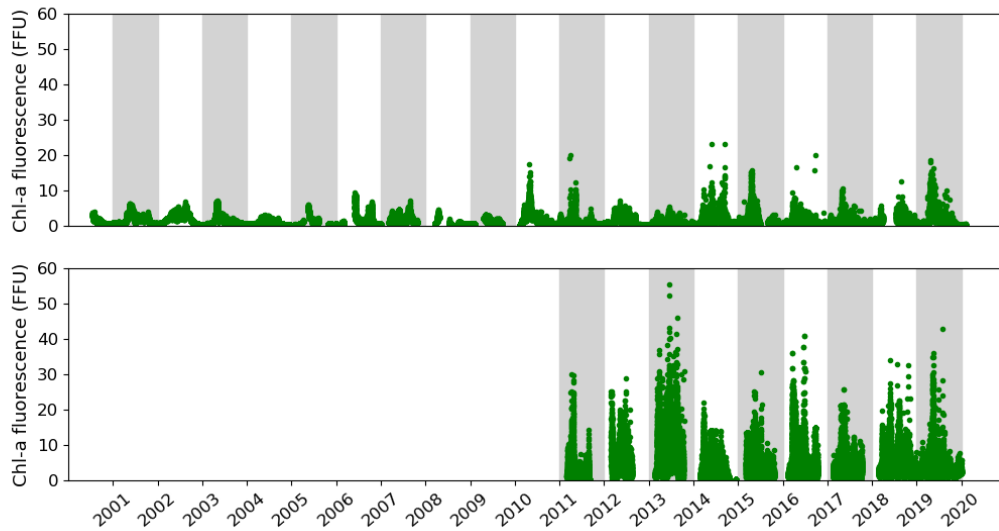
965
966
967
968
969

Figure 2: Importance of the Quenching effect on Chl-*a* fluorescence is represented by COAST-HF-Iroise data from 2000 to 2019. The standard deviation is represented by vertical black bars. The dashed lines represent the beginning and end of the selected values for the rest of the study from 10 pm to 5 am.



970
971
972
973

Figure 3: Example of detection of the start (red line) and end (blue line) of the phytoplankton growing period in 2001 at COAST-HF-Iroise. The threshold value - median of slopes - is represented by a dotted grey line.



974
975
976
977
978
979

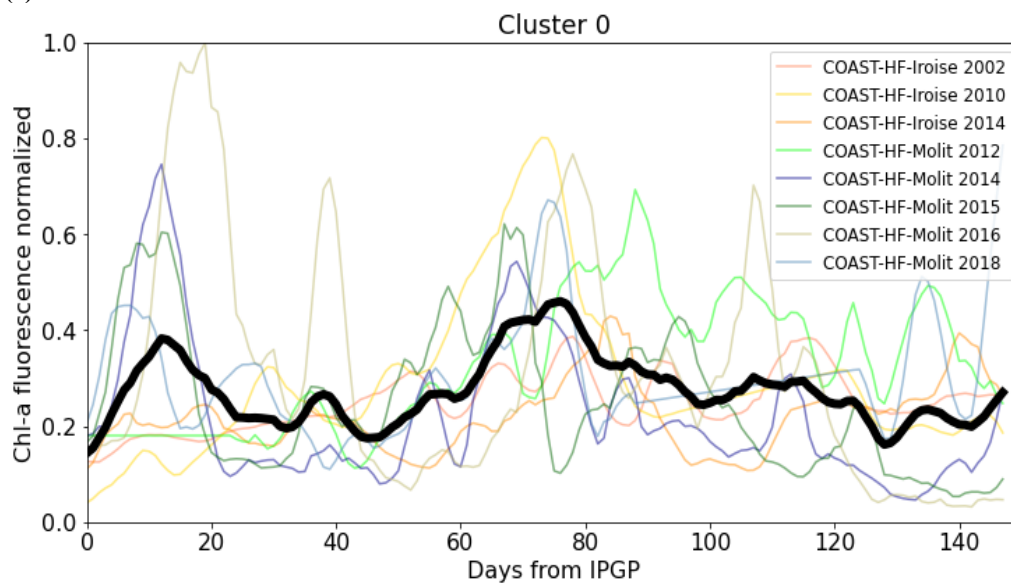
Figure 4: Temporal changes in the *in situ* Chl-*a* fluorescence measured in the Bay of Brest (top) and the Bay of Vilaine (bottom).

	Start date (Day of year)	End date (Day of year)	Duration (Days)	Cumulative Chl- <i>a</i> fluorescence (FFU)
	<i>Min - Median - Max</i>	<i>Min - Median - Max</i>	<i>Min - Median - Max</i>	<i>Min - Median - Max</i>
Bay of Brest (2001-2019)	50 - 69 - 102	253 - 274 - 308	165 - 200 - 256	217 - 364 - 567
Bay of Vilaine (2011-2019)	53 - 68 - 93	218 - 269 - 316	165 - 179 - 239	276 - 582 - 1406

980
981
982
983
984
985
986

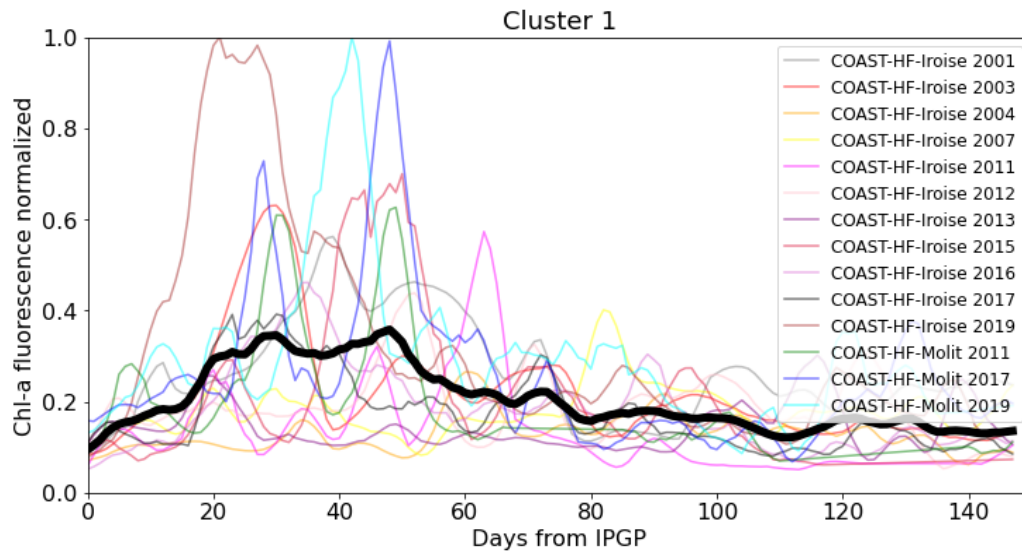
Table 2: Global characteristics of the phytoplankton growing period in the Bay of Brest and in the Bay of Vilaine.

(a)



987
988
989

990 (b)
991



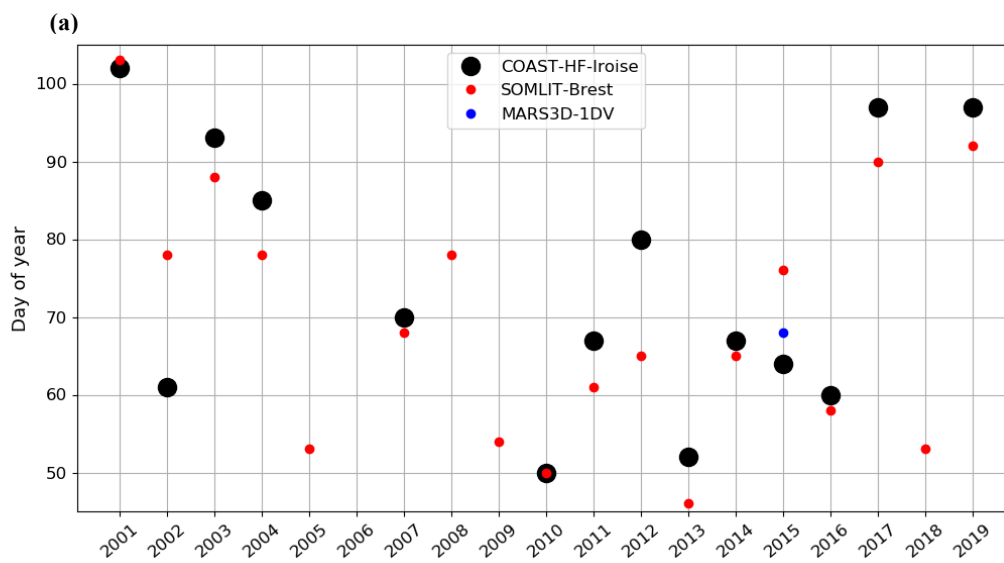
992
993
994
995
996
997
998

Figure 5: (a) Cluster 0 and (b) cluster 1 representative of the patterns of the phytoplankton growing period observed in both bays. The median pattern is drawn in bold.

Year	2001	2002	2003	2004	2005	2006	2007	2008	2009	2010	2011	2012	2013	2014	2015	2016	2017	2018	2019
Bay of Brest COAST-HF-Iroise	1	0	1	1			1			0	1	1	1	0	1	1	1		1
Bay of Vilaine COAST-HF-Molit											1	0	X	0	0	0	1	0	1

999
1000
1001
1002
1003
1004
1005

Table 3: Cluster group assigned to each annual phytoplankton growing period on both sites. Grey boxes represent years with missing data. The cross represents the year 2013 of the Bay of Vilaine not considered.



1006
1007
1008
1009

(b)

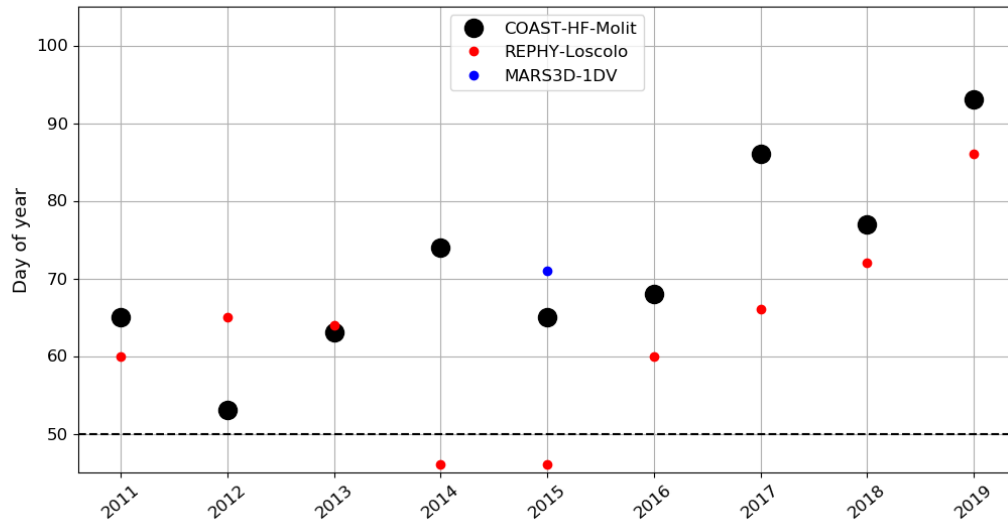
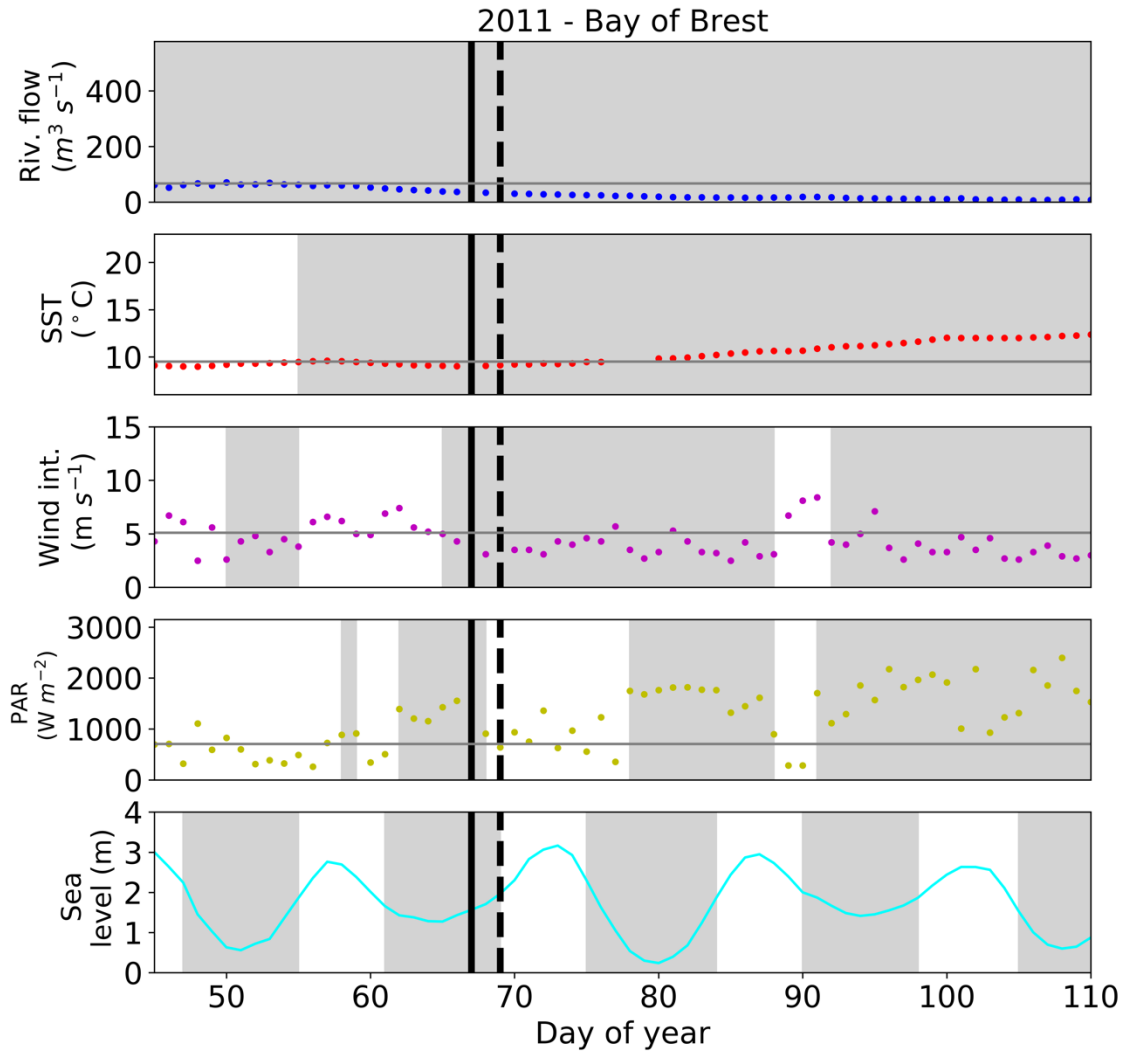


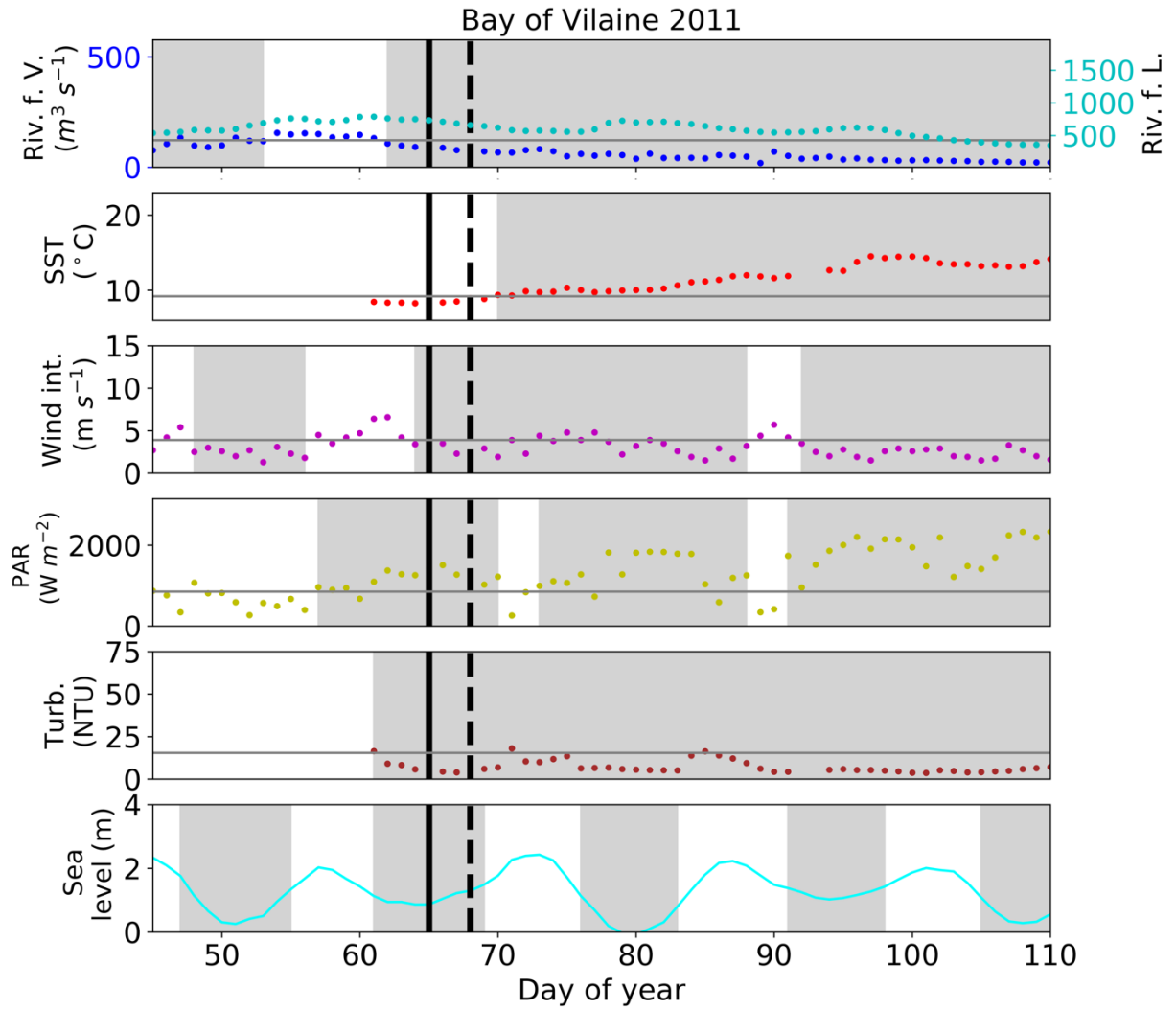
Figure 6: Changes in the IGP date in (a) the Bay of Brest and (b) the Bay of Vilaine are determined with high-frequency time series (black circles), low-frequency time series (red circles) and with the model (blue circle). The dotted black line represents the date of the COAST-HF-Molit buoy deployment.

1010
 1011
 1012
 1013
 1014
 1015
 1016
 1017
 1018
 1019
 1020
 1021
 1022
 1023
 1024
 1025
 1026
 1027
 1028
 1029
 1030
 1031
 1032
 1033
 1034
 1035
 1036
 1037
 1038
 1039
 1040
 1041
 1042
 1043
 1044
 1045
 1046
 1047
 1048
 1049
 1050
 1051
 1052
 1053
 1054
 1055
 1056
 1057
 1058



1060
 1061
 1062
 1063
 1064
 1065
 1066
 1067
 1068
 1069
 1070
 1071
 1072
 1073
 1074
 1075
 1076
 1077
 1078
 1079
 1080
 1081
 1082

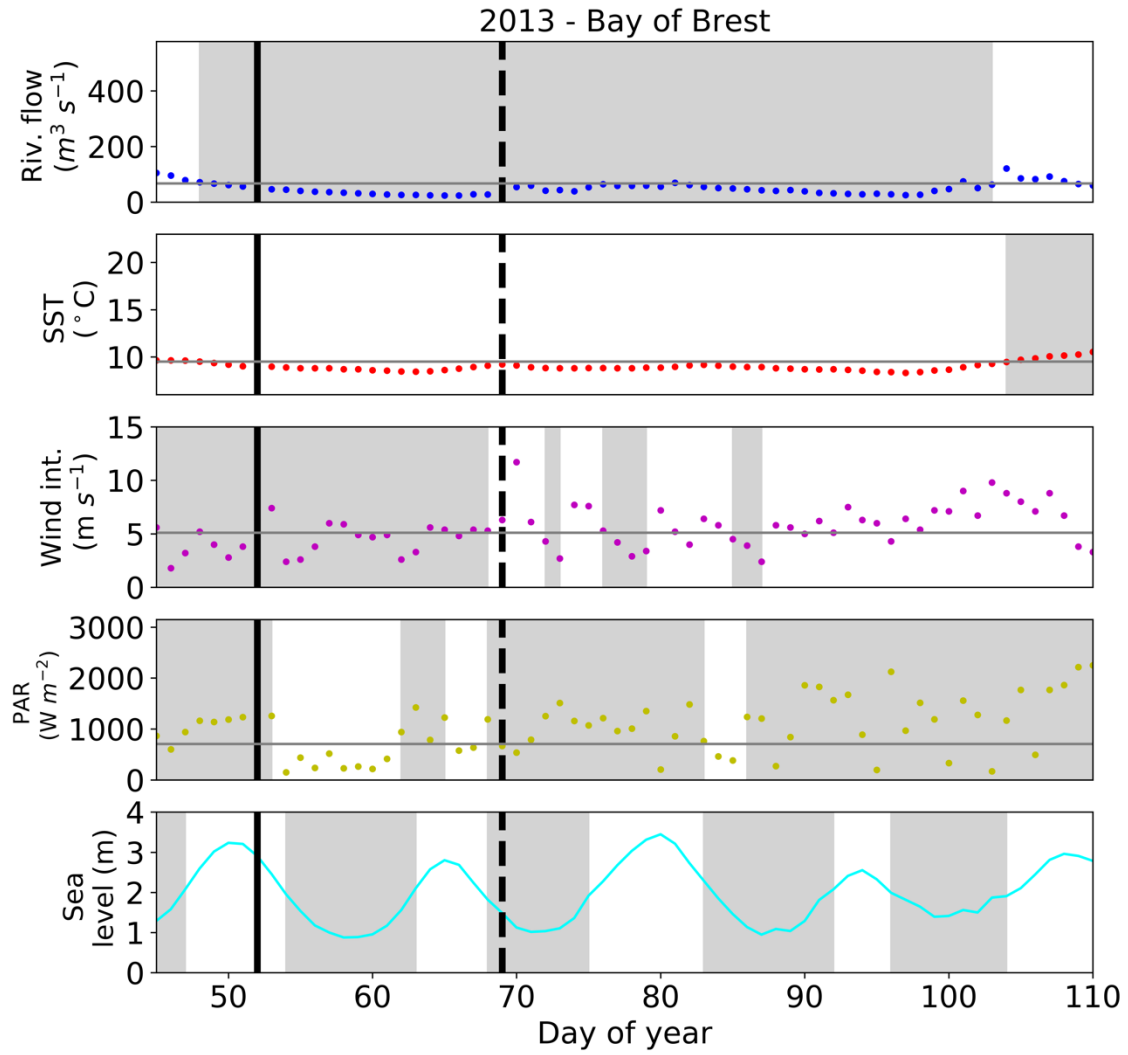
1083 (b)



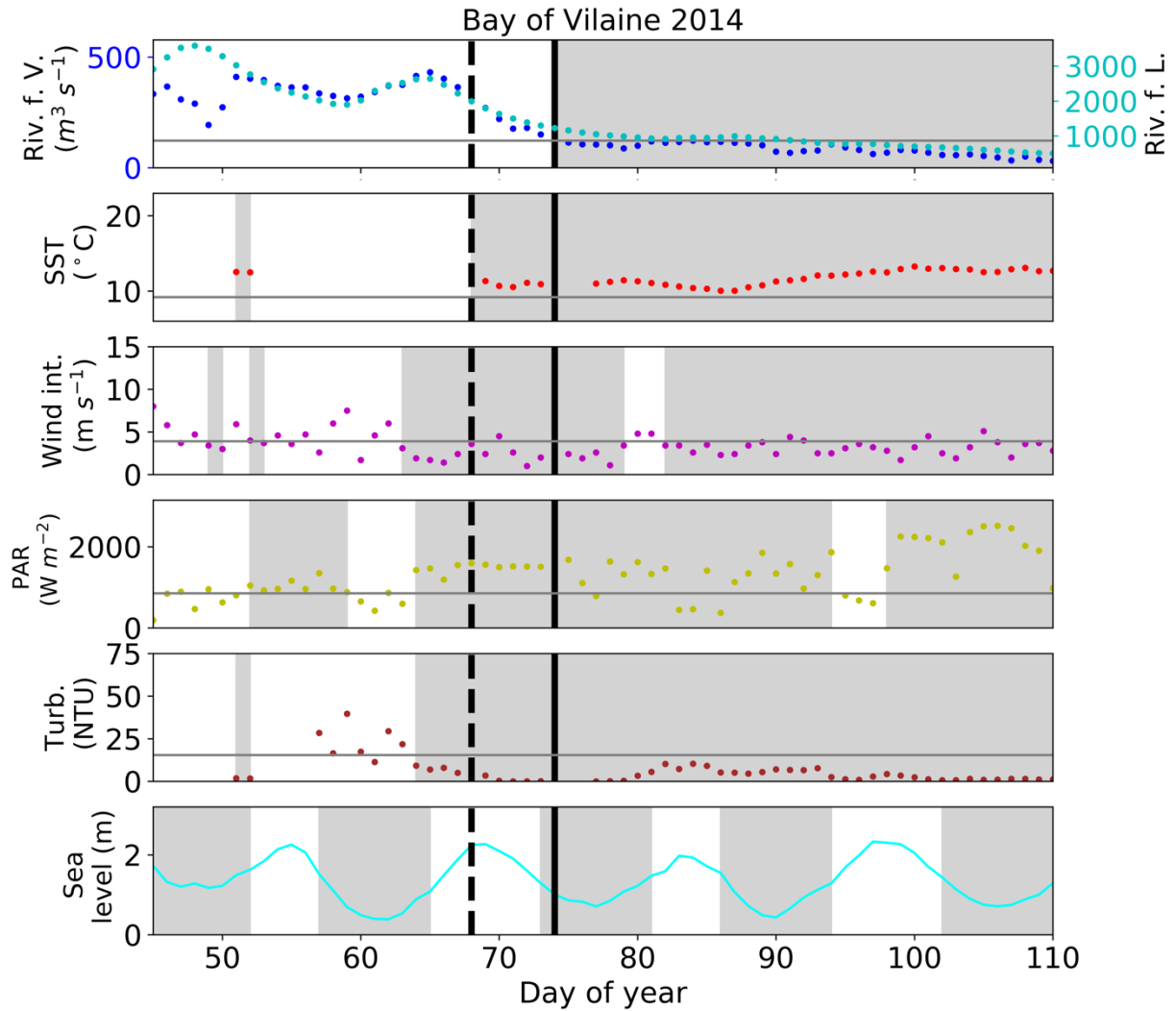
1084
1085
1086
1087
1088
1089
1090
1091
1092
1093
1094
1095
1096
1097
1098
1099
1100
1101
1102
1103
1104
1105
1106

1107
1108
1109

(c)



1110
1111
1112
1113
1114
1115
1116
1117
1118
1119
1120
1121
1122
1123
1124
1125
1126
1127
1128
1129
1130



1132
 1133
 1134
 1135
 1136
 1137
 1138
 1139
 1140
 1141
 1142

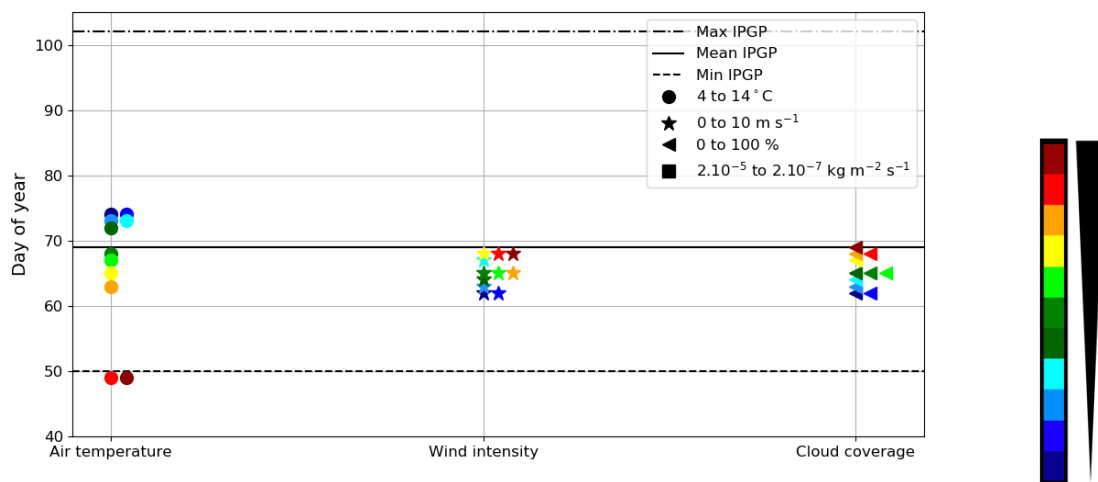
Figure 7: IPGP dates and environmental drivers: flow of the Aulne, Vilaine and Loire rivers, Sea Surface Temperature (SST), wind intensity, PAR, turbidity and sea level at high tide. Illustrations in 2011 for a mean IPGP date in (a) the Bay of Brest and (b) the Bay of Vilaine; in 2013 for an early IPGP date in (c) the Bay of Brest; in 2014 for a late IPGP date in (d) the Bay of Vilaine. The mean IPGP date of each bay is represented by a dotted black line and the IPGP date of the year is represented by a straight black line. Thresholds of each environmental driver are represented by grey vertical lines corresponding to the mean conditions calculated 30 days around the IPGP date. Grey areas are time periods favorable to IPGP.

	Bay of Brest (2001-2019)	Bay of Vilaine (2011-2019)
	<i>Min - Median - Max</i>	<i>Min - Median - Max</i>
River flow (m ³ s ⁻¹)	13 - 46 - 100	36 - 96 - 205
SST (°C)	8 - 10 - 12	8 - 10 - 11
Wind intensity (m s ⁻¹)	1 - 3 - 6	1 - 3 - 4
PAR (W m ⁻²)	915 - 1373 - 2220	814 - 1341 - 1939
Turbidity (NTU)	1 - 7 - 21	0 - 7 - 22
Sea level (m)	0.5 - 1.6 - 2.9	0.6 - 0.9 - 1.6
PO₄ (μmol/L)	0.1 - 0.4 - 0.6	0.1 - 0.8 - 1.4
DIN (μmol/L)	8 - 20 - 38	25 - 57 - 244
Si(OH)₄ (μmol/L)	4 - 8 - 16	8 - 38 - 112

1143
1144
1145
1146
1147
1148
1149

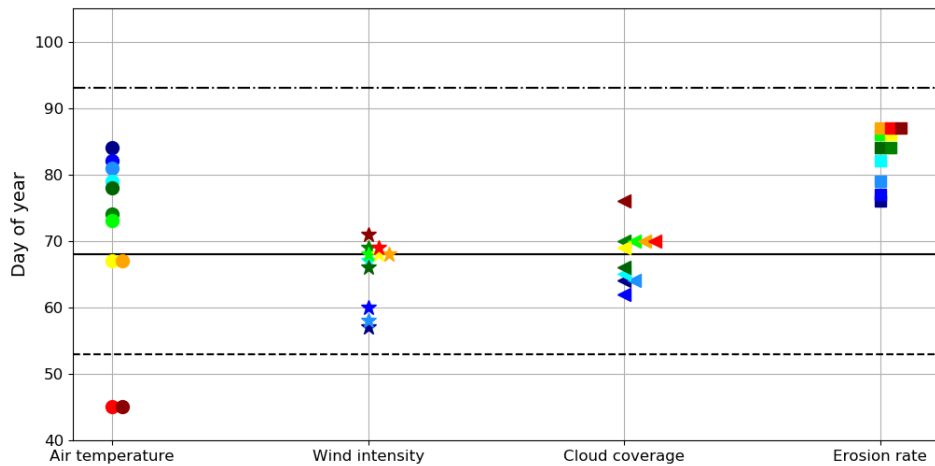
Table 4: Characteristics of environmental drivers at the date of IPGP in the Bay of Brest and in the Bay of Vilaine.

(a)



1150
1151
1152

(b)



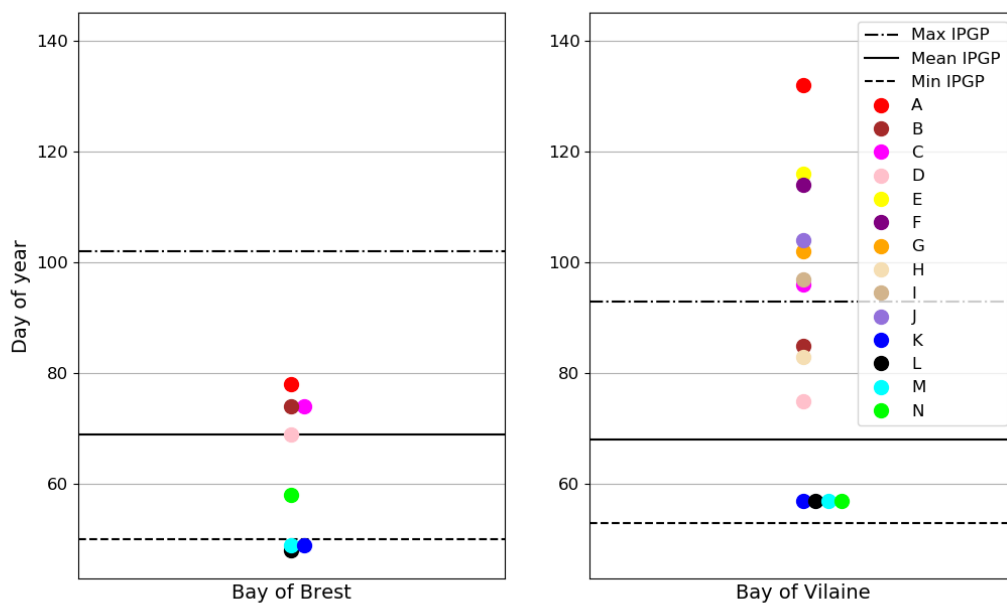
1153
1154
1155
1156
1157
1158
1159
1160

Figure 8: Impact of the variation of environmental drivers on the date of IPGP in (a) the Bay of Brest and (b) the Bay of Vilaine. Steps of: 1°C for the air temperature, 1 m s⁻¹ for the wind intensity, 10 % for the cloud coverage and 0.0000036 kg m⁻² s⁻¹ for the erosion rate equivalent to a variation of suspended matter between 0.02 and 0.08 mg L⁻¹ at IPGP.

Experiment	Air temperature (°C)	Wind intensity (m s ⁻¹)	Cloud coverage (%)	Erosion rate (kg m ⁻² s ⁻¹)	Simulated IPGP Bay of Brest (days)	Simulated IPGP Bay of Vilaine (days)
1	4	3	70	2.10 ⁻⁶	+5	+16
2	14	3	70	2.10 ⁻⁶	-20	-23
3	10	0	70	2.10 ⁻⁶	-1	-11
4	10	10	70	2.10 ⁻⁶	-7	+3
5	10	3	0	2.10 ⁻⁶	=	-4
6	10	3	100	2.10 ⁻⁶	-7	+8
7	10	3	70	2.10 ⁻⁷		+8
8	10	3	70	2.10 ⁻⁵		+19
A	4	10	100	2.10 ⁻⁵	+9	+64
B	4	10	70	2.10 ⁻⁶	+5	+17
C	4	3	100	2.10 ⁻⁶	+5	+28
D	10	10	100	2.10 ⁻⁶	=	+6
E	4	10	70	2.10 ⁻⁵		+48
F	4	3	100	2.10 ⁻⁵		+46
G	10	10	100	2.10 ⁻⁵		+34
H	10	3	100	2.10 ⁻⁵		+19
I	10	10	70	2.10 ⁻⁵		+29
J	4	3	70	2.10 ⁻⁵		+36
K	14	0	0	2.10 ⁻⁷	-20	-11
L	14	0	70	2.10 ⁻⁷	-21	-11
M	14	3	0	2.10 ⁻⁷	-20	-11
N	10	0	0	2.10 ⁻⁷	-11	-11

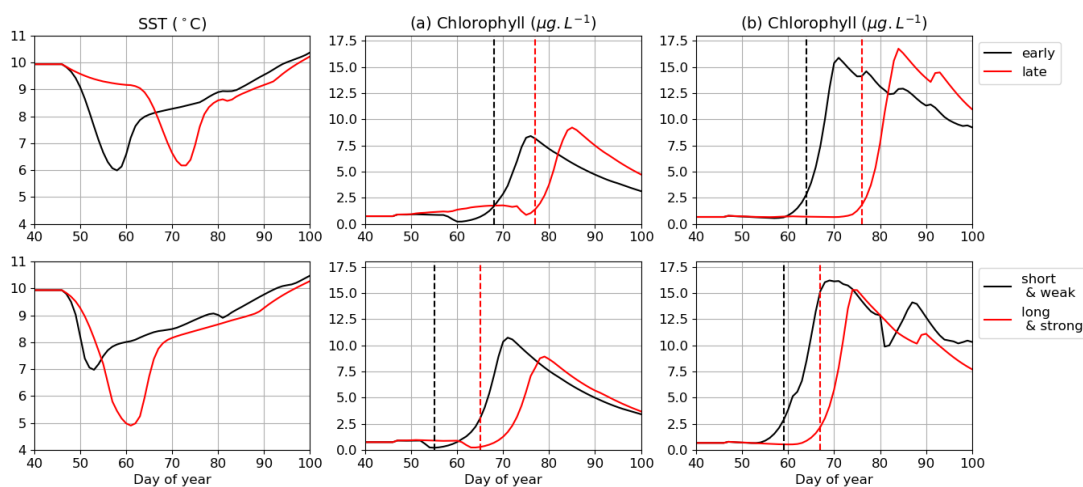
1161
1162
1163
1164

Table 5: Assumptions are explored in the 1DV model for environmental parameters independently (1-8) and with combined effect (A-N) with the modified values (grey background) and text in bold for the Bay of Brest only (+ for later IPGP, - for earlier IPGP, = for equal IPGP) with IPGP equal the mean observed IPGP of day 68.



1165
1166
1167
1168

Figure 9: Influence of combined environmental parameters for the MARS-1DV model in both bays (Bay of Brest - left and Bay of Vilaine - right) with detailed experiments in Table 2.



1169

1170
1171
1172
1173
1174
1175
1176
1177
1178
1179

Figure 10: Impact of cold spells on the IPGP date simulated in (a) the Bay of Brest and (b) the Bay of Vilaine. Four conditions of cold spells are explored: an early (mid-February), a late (end of February), a short (8 days) and a long (20 days). The IPGP dates are represented by dotted lines.